Supplementary Information

Ring-opening polymerisation of *L*- and *rac*-lactide using group 4 permethylpentalene aryloxides and alkoxides

Zoë R. Turner, Jessica V. Lamb, Thomas P. Robinson, Dipa Mandal, Jean-Charles Buffet and Dermot O'Hare (*)

† Chemistry Research Laboratory, Department of Chemistry, University of Oxford, 12 Mansfield Road, OX1 3TA Oxford, United Kingdom. Tel: +44(0) 1865 272686; E-mail: dermot.ohare@chem.ox.ac.uk

Table of Contents

1. General experimental details

1.1 Air- and moisture-sensitive compounds

Air- and moisture-sensitive compounds were handled under an inert N_2 atmosphere, using standard Schlenk line techniques and an MBraun Unilab glove box when required.

1.2 Commercially supplied reagents

Sublimed KO^{t}Bu (Sigma Aldrich) was used as supplied.

1.3 Solvent preparation

Pentane, hexane, toluene and benzene were dried using an MBraun SPS-800 solvent purification system, stored over a potassium mirror and degassed under partial vacuum before use. Deuterated solvents were dried over K (benzene-d_6) or CaH_2 (tetrahydrofuran-d_8), distilled under static vacuum, freeze-thaw degassed and stored over pre-activated 4 Å molecular sieves under N_2.

1.4 Synthesis of literature compounds

[Pn*ZrCl$_2$]·LiCl·thf$_2$,[1] Pn*ZrCp(Cl),[2] Pn*TiCp(Cl),[2] Pn*ZrCp^{Me}(Cl),[3] KO-2,6-Me-C$_6$H$_3$,[4] K(O-2,6-^{i}Pr-C$_6$H$_3$),[5] KO-2,6-^{t}Bu-C$_6$H$_3$[5] and KO-2,6-^{t}Bu-4-Me-C$_6$H$_2$[6] were synthesised according to literature procedures. KO-4-OMe-C$_6$H$_4$ was synthesised according to a modified literature procedure.[5]

1.5 Solution phase NMR spectroscopy

NMR spectroscopy samples of air- and moisture-sensitive compounds were prepared in a glove box and sealed in 5 mm Young's tap NMR tubes. ^{1}H NMR and ^{13}C{^{1}H} spectra were recorded on either a Bruker Avance III HD nanobay 400 MHz or Bruker Avance III 500 MHz NMR spectrometer. All spectra were recorded at 298 K and referenced internally to the residual *protio* solvent peak. All spectra are reported relative to tetramethylsilane (δ = 0 ppm). Two dimensional ^{1}H-^{1}H and ^{13}C-^{1}H correlation experiments were used, when necessary, to confirm ^{1}H and ^{13}C assignments.

Permethylpentalene (Pn*) methyl and carbon resonances are assigned according to:

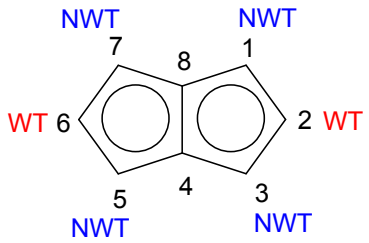

Where NWT denotes "non-wingtip" and WT denotes "wingtip"

1.6 Elemental analysis

Samples were prepared in a glove box and sealed in glass vials under nitrogen. CHN analyses were carried out in duplicate by Mr Stephen Boyer, London Metropolitan University.

1.7 Gel-permeation chromatography (GPC)

Gel permeation chromatography studies were performed using a Shimadzu LC-20AD instrument at 40 °C. Two Mixed Bed PSS SDV linear S columns were used in series, with THF as the eluent and a flow rate of 1 mL min^{-1}. The instrument was calibrated using narrow M_n polystyrene standards (correction factor of 0.58) and polymer samples were dissolved in SEC grade THF and filtered prior to analysis.[7]

1.8 MALDI-TOF mass spectrometry

Matrix-assisted laser desorption/ionisation time of flight spectra were collected by Dr Victor Mikhailov (University of Oxford) using a Bruker MALDI Autoflex TOF MS. Samples were run using a DCTB matrix. The DCTB matrix was prepared by mixing 10 µL of sample with 10 µL DCTB (40 mg mL^{-1} in THF) and 2.5 µL KTFA (5 mg mL^{-1} in THF). 1.5 µL of the mixed solutions were spotted on the MALDI plate and dried prior to the run.

2. Representative NMR spectra

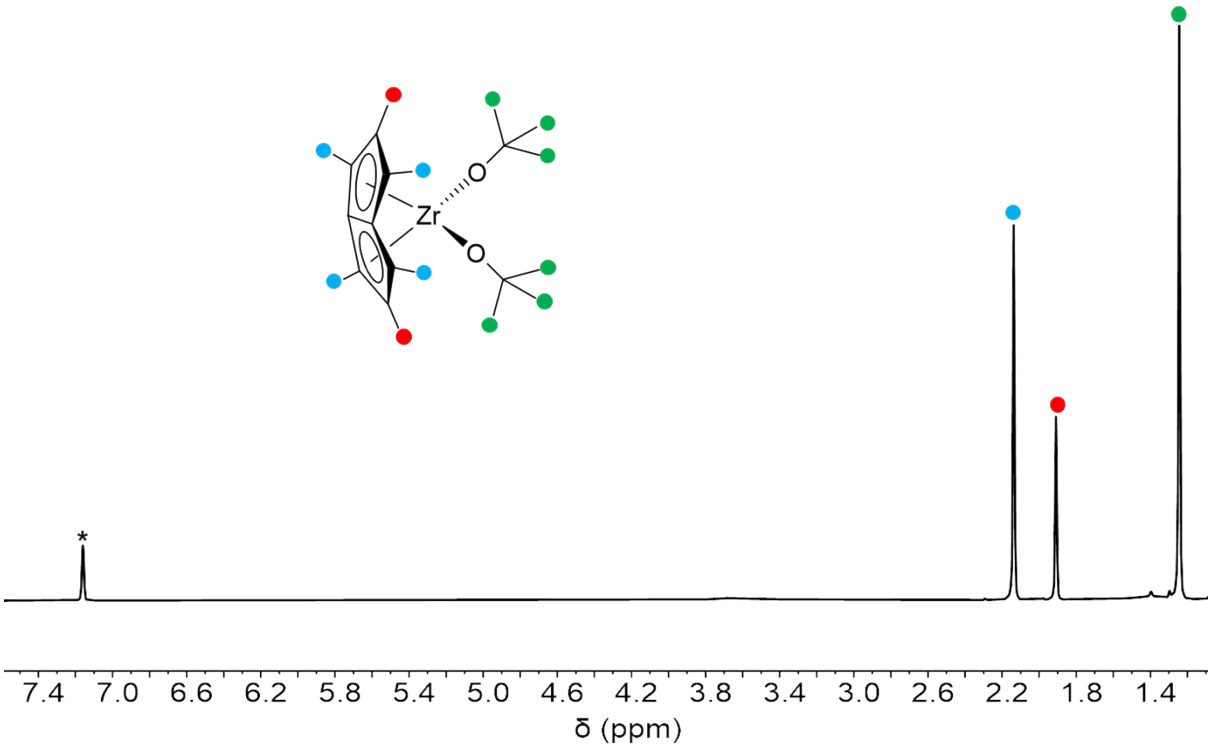

Fig. S1. ^{1}H NMR spectrum (benzene-d_6 (*), 400 MHz, 298 K) of Pn*Zr(O^{t}Bu)$_2$ (**1**).

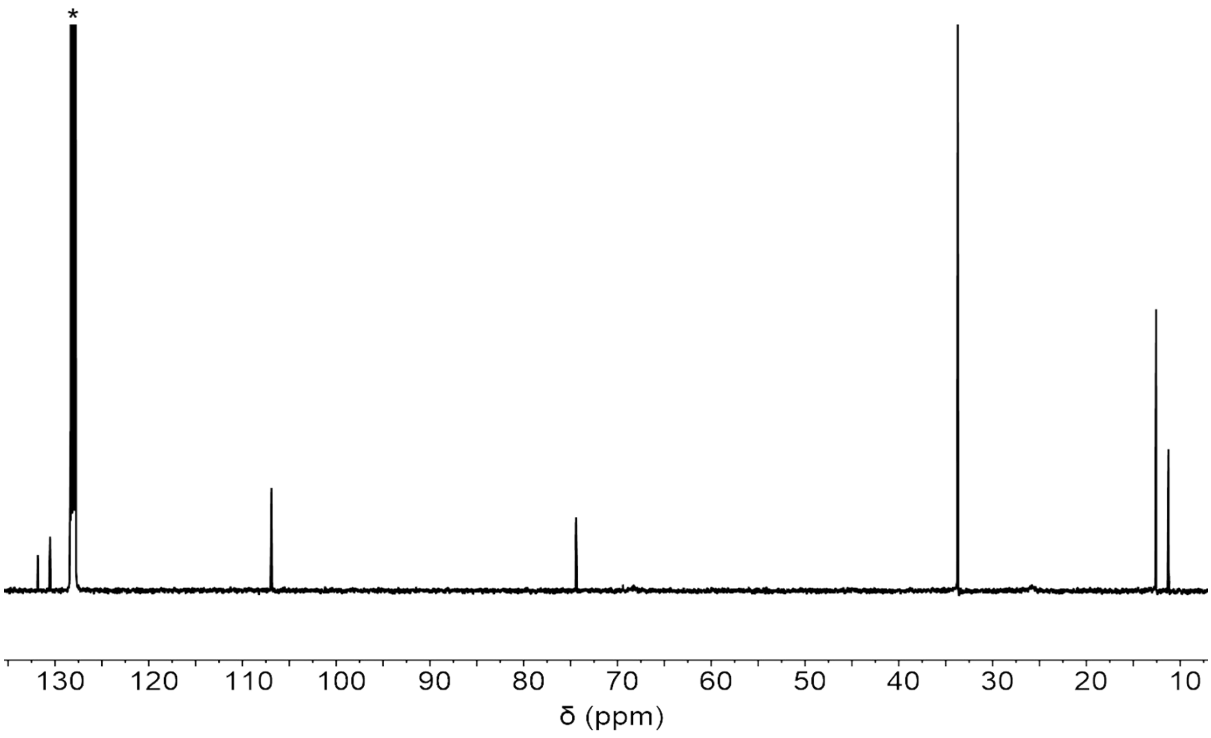

Fig. S2. ^{13}C{^{1}H} NMR spectrum (benzene-d_6 (*), 125 MHz, 298 K) of Pn*Zr(O^{t}Bu)$_2$ (**1**).

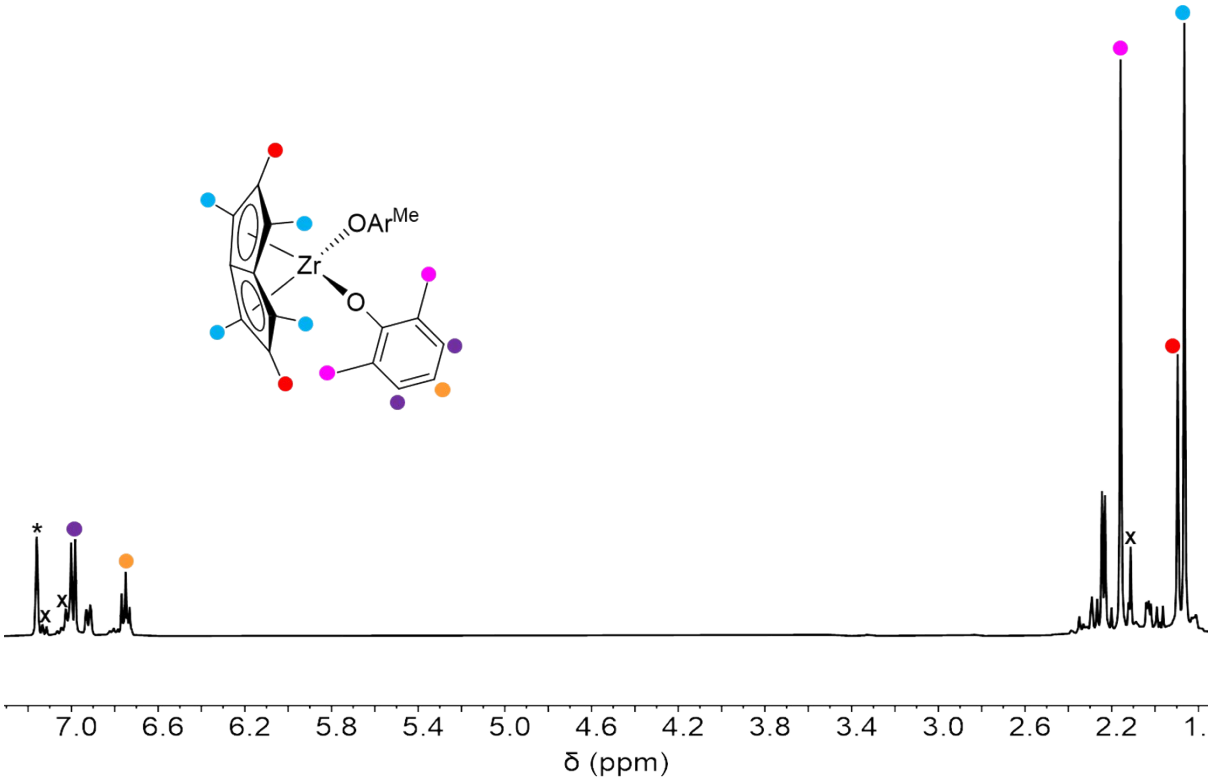

Fig. S3. ^{1}H NMR spectrum (benzene-d_6 (*), 400 MHz, 298 K) of Pn*Zr(O-2,6-Me-C_6H_3)$_2$ (**2**). x is residual toluene.

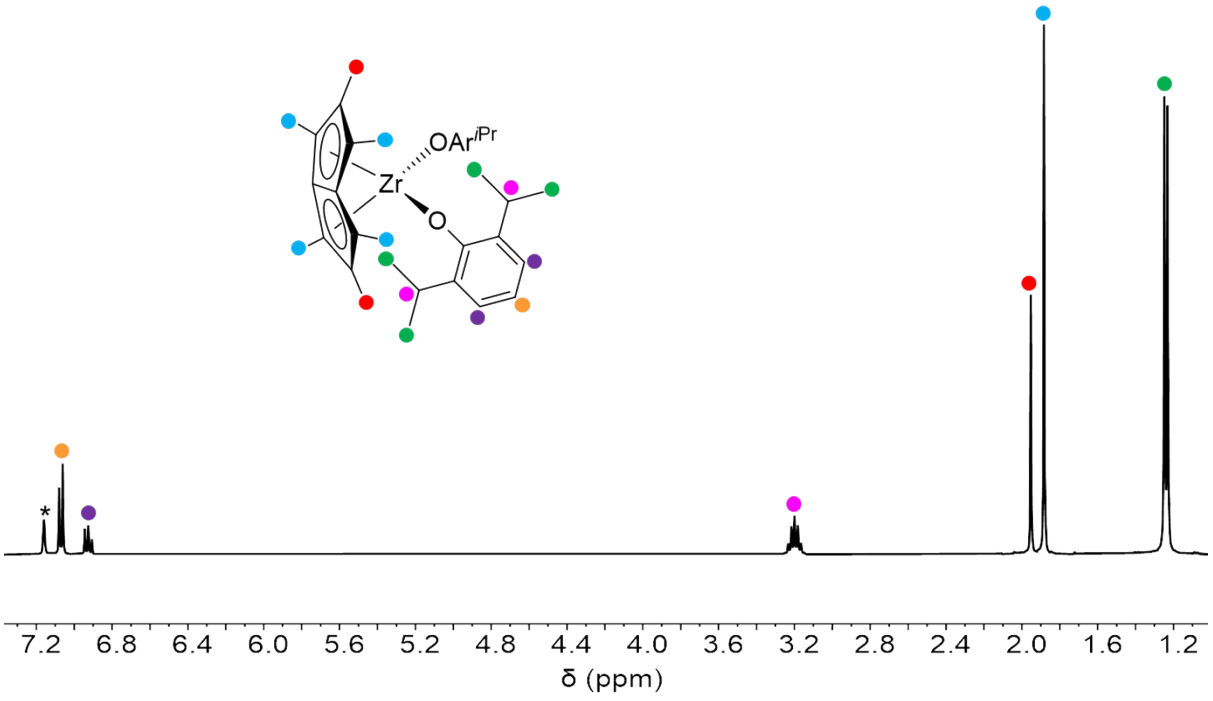

Fig. S4. ^{1}H NMR spectrum (benzene-d_6 (*), 400 MHz, 298 K) of Pn*Zr(O-2,6-^{i}Pr-C_6H_3)$_2$ (**3**).

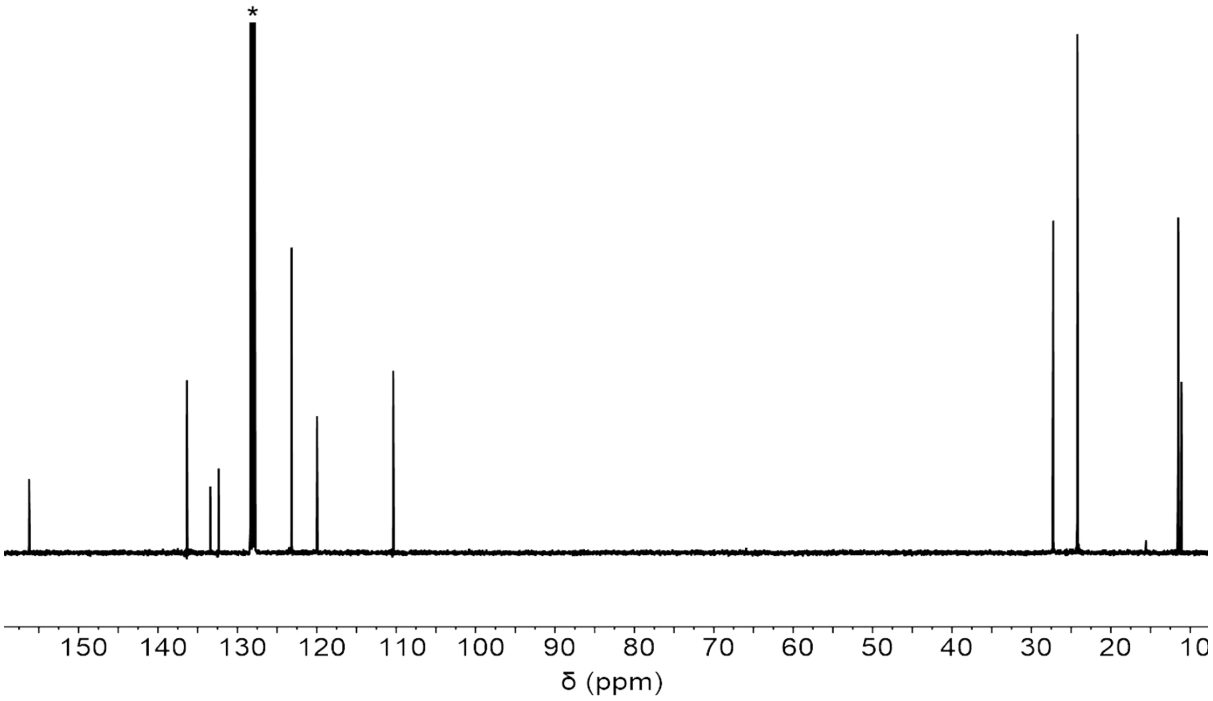

Fig. S5. $^{13}C\{^{1}H\}$ NMR spectrum (benzene-d_6 (*), 101 MHz, 298 K) of Pn*Zr(O-2,6-^{i}Pr-C_6H_3)$_2$ (**3**).

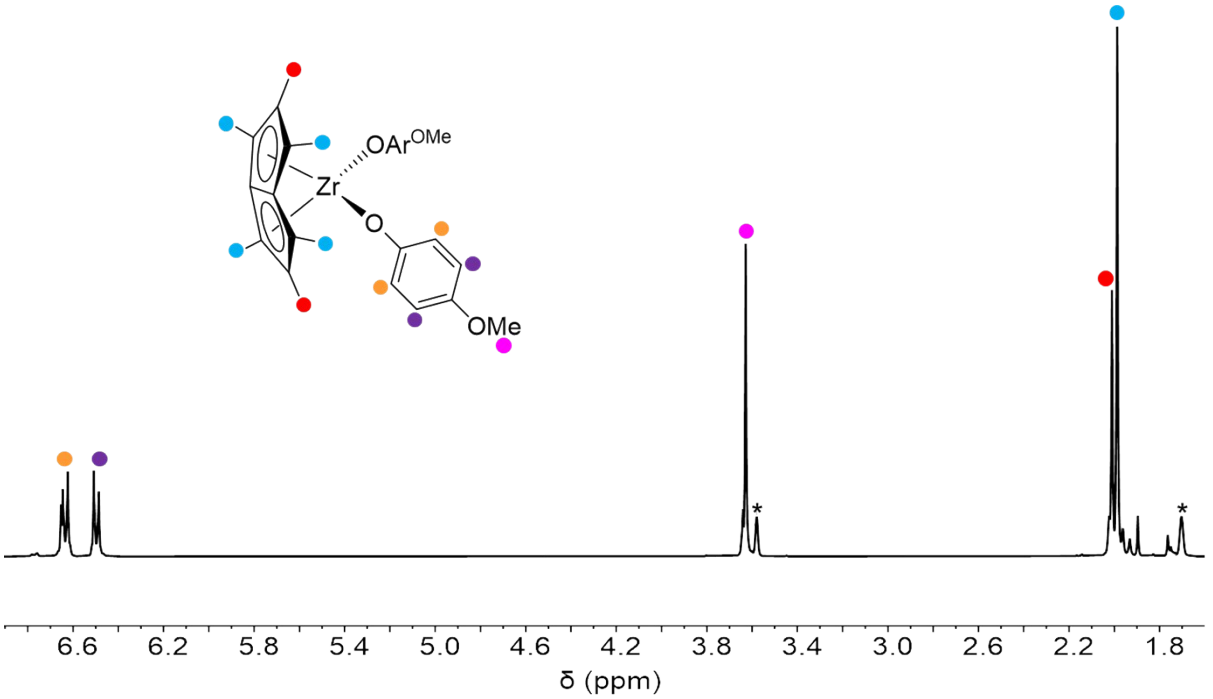

Fig. S6. ^{1}H NMR spectrum (tetrahydrofuran-d_8 (*), 400 MHz, 298 K) of Pn*ZrCl(O-4-OMe-C_6H_4) (**4**).

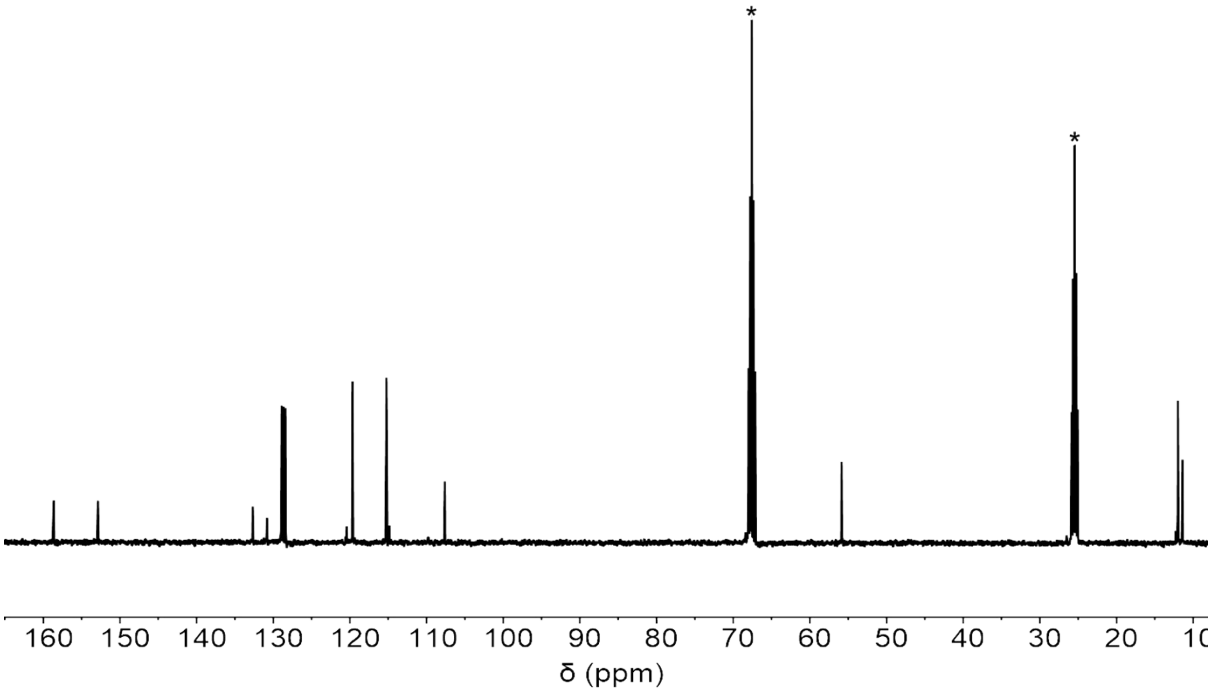

Fig. S7. $^{13}C\{^{1}H\}$ NMR spectrum (tetrahydrofuran-d_8 (*), 101 MHz, 298 K) of Pn*ZrCl(O-4-OMe-C_6H_4) (**4**).

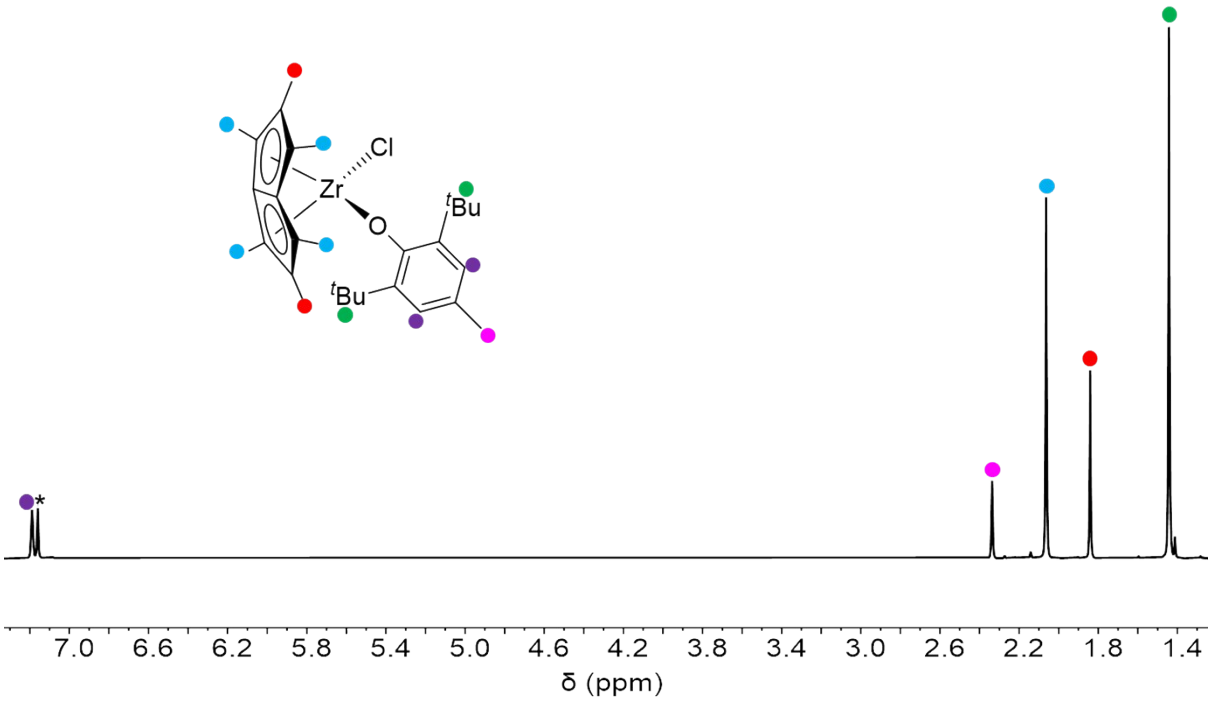

Fig. S8. ^{1}H NMR spectrum (benzene-d_6 (*), 400 MHz, 298 K) of Pn*ZrCl(O-2,6-^{t}Bu-4-Me-C_6H_2) (**6**).

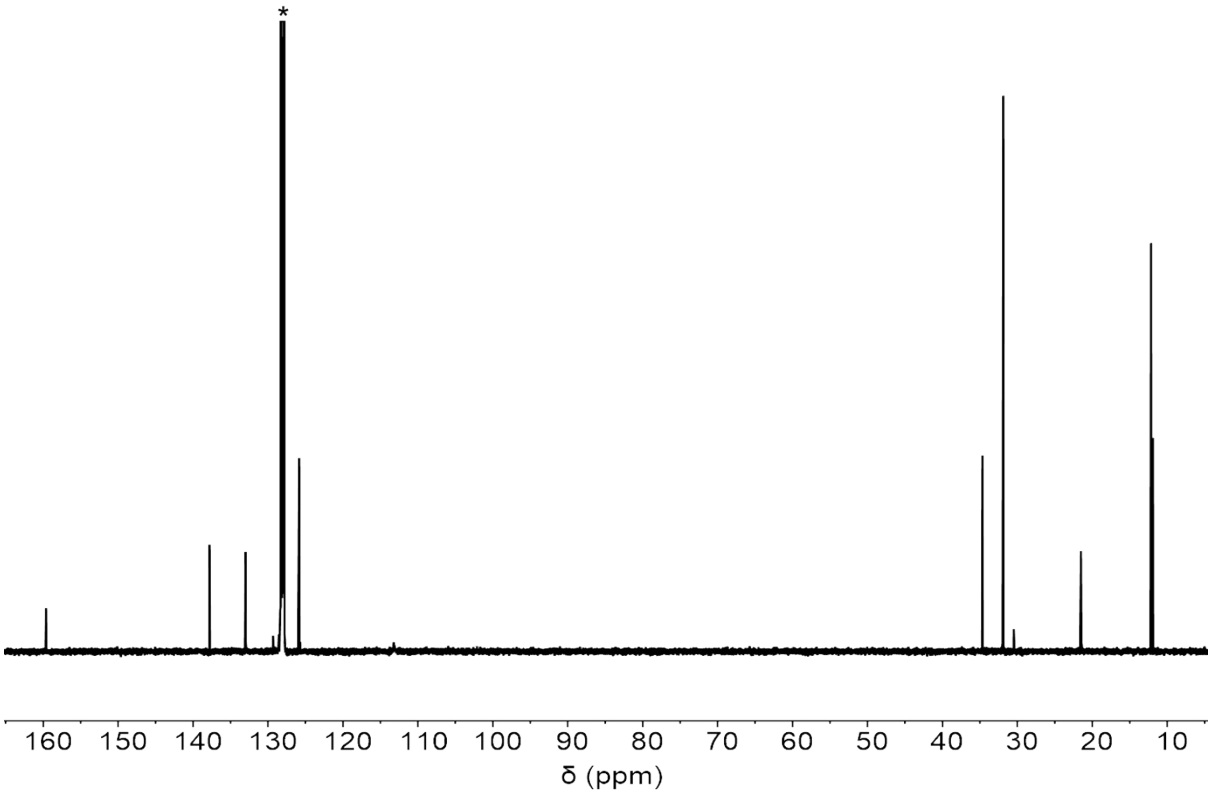

Fig. S9. $^{13}C\{^{1}H\}$ NMR spectrum (benzene-d_6 (*), 101 MHz, 298 K) of Pn*ZrCl(O-2,6-^{t}Bu-4-Me-C_6H_2) (**6**).

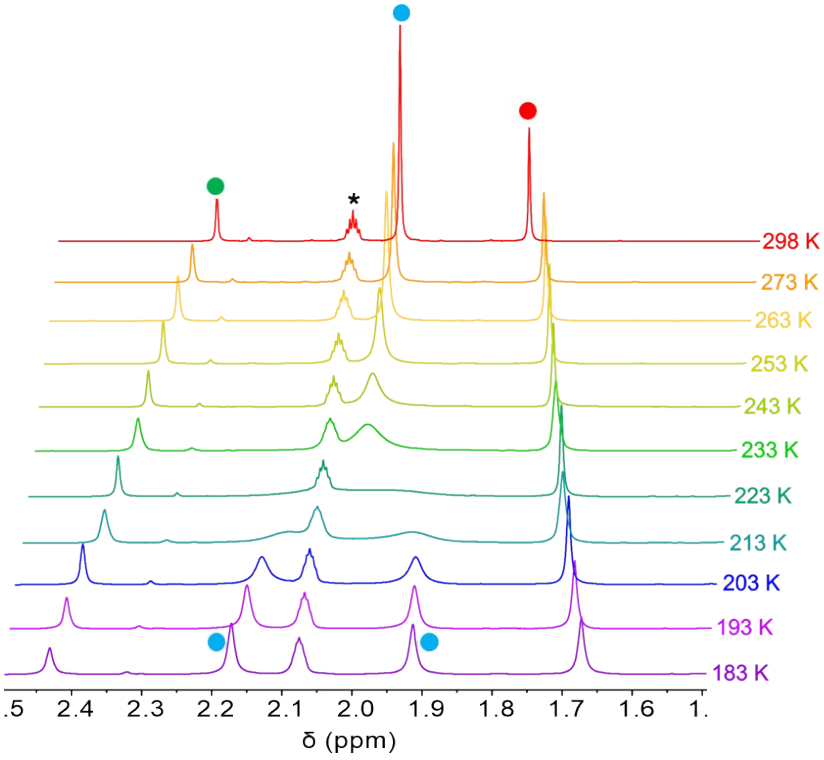

Fig. S10. Variable temperature ^{1}H NMR spectra (toluene-d_8 (*), 500 MHz) of Pn*ZrCl(O-2,6-^{t}Bu-4-Me-C_6H_2) (**6**) between 183 and 298 K.

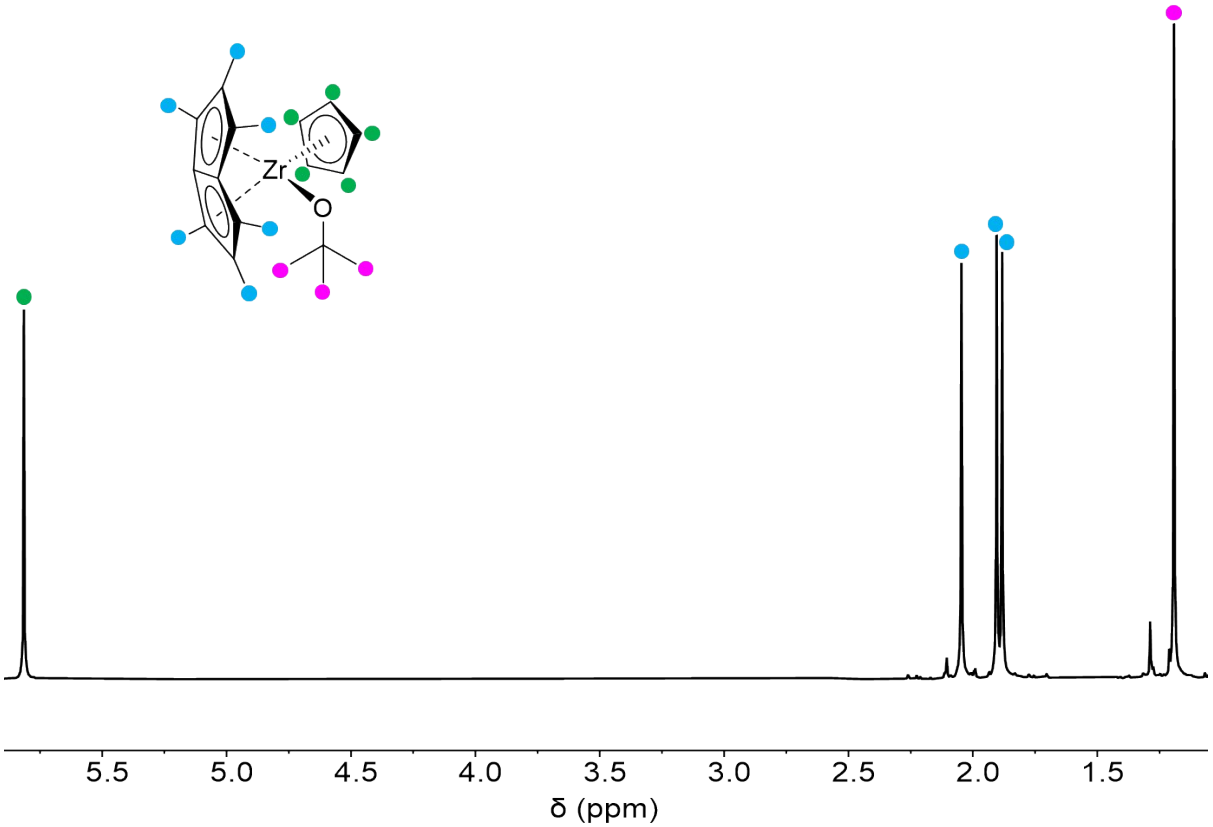

Fig. S11. ^{1}H NMR spectrum (benzene-d_6 (*), 500 MHz, 298 K) of Pn*ZrCp(O^{t}Bu) (**7**).

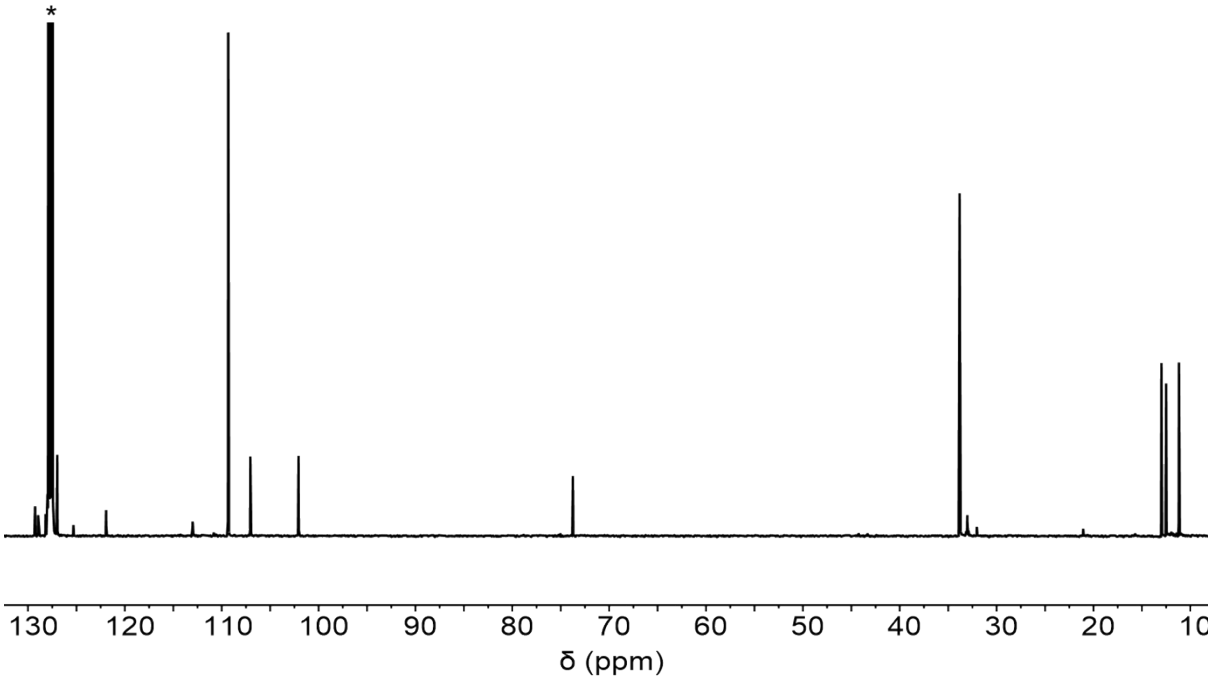

Fig. S12. $^{13}C\{^{1}H\}$ NMR spectrum (benzene-d_6 (*), 125 MHz, 298 K) of Pn*ZrCp(O^{t}Bu) (**7**).

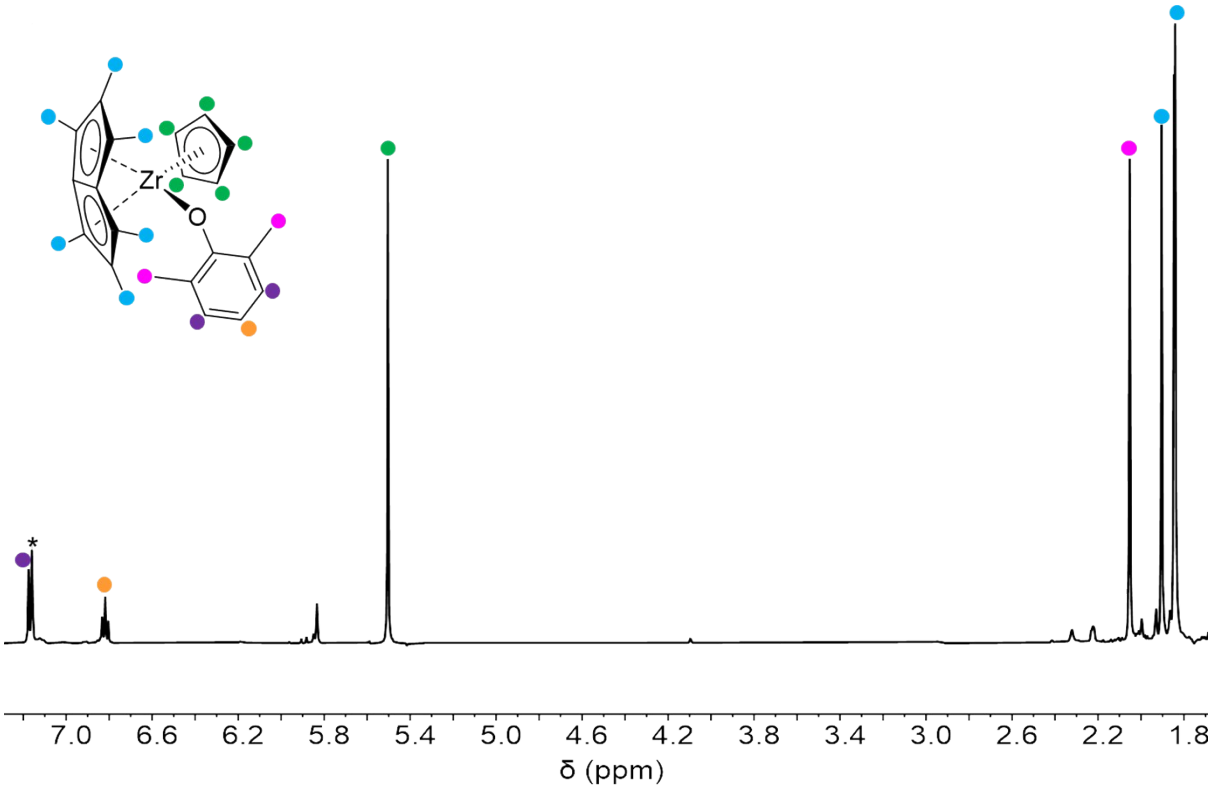

Fig. S13. ^{1}H NMR spectrum (benzene-d_6 (*), 500 MHz, 298 K) of Pn*ZrCp(O-2,6-Me-C_6H_3) (**8**).

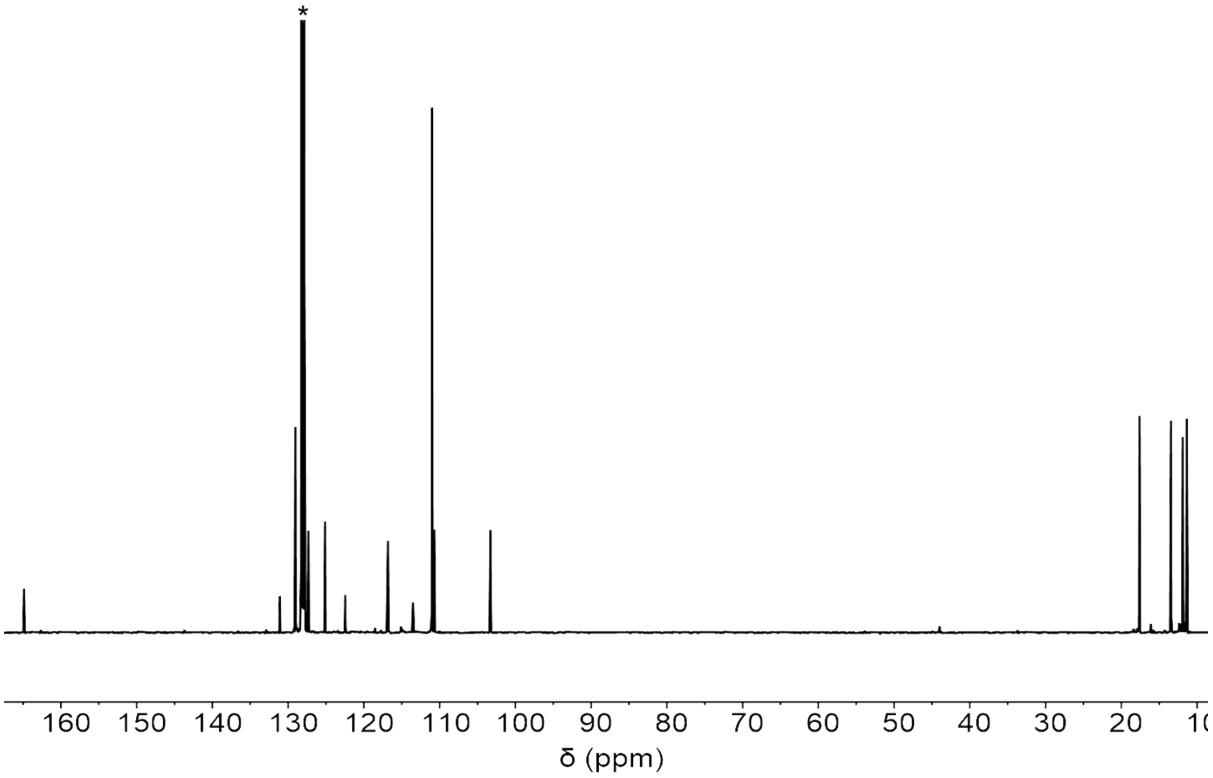

Fig. S14. $^{13}C\{^{1}H\}$ NMR spectrum (benzene-d_6 (*), 125 MHz, 298 K) of Pn*ZrCp(O-2,6-Me-C_6H_3) (**8**).

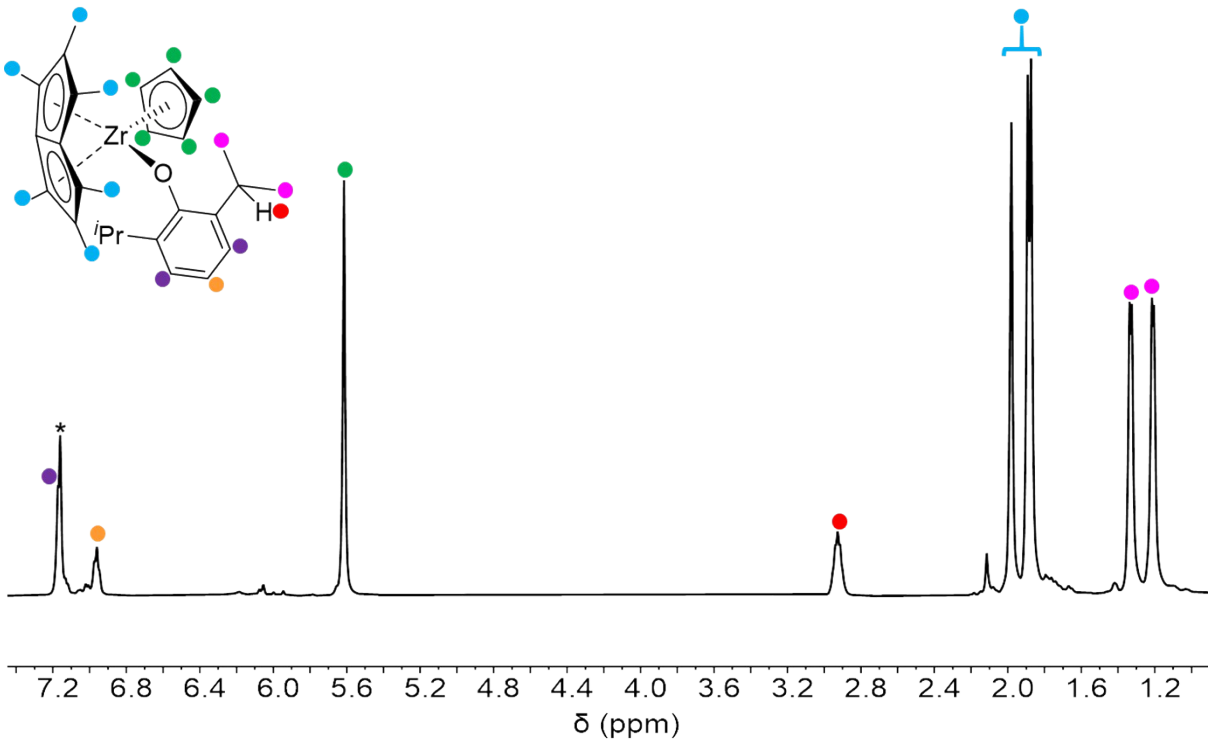

Fig. S15. ^{1}H NMR spectrum (benzene-d_6 (*), 500 MHz, 298 K) of Pn*ZrCp(O-2,6-^{i}Pr-C_6H_3) (**9**).

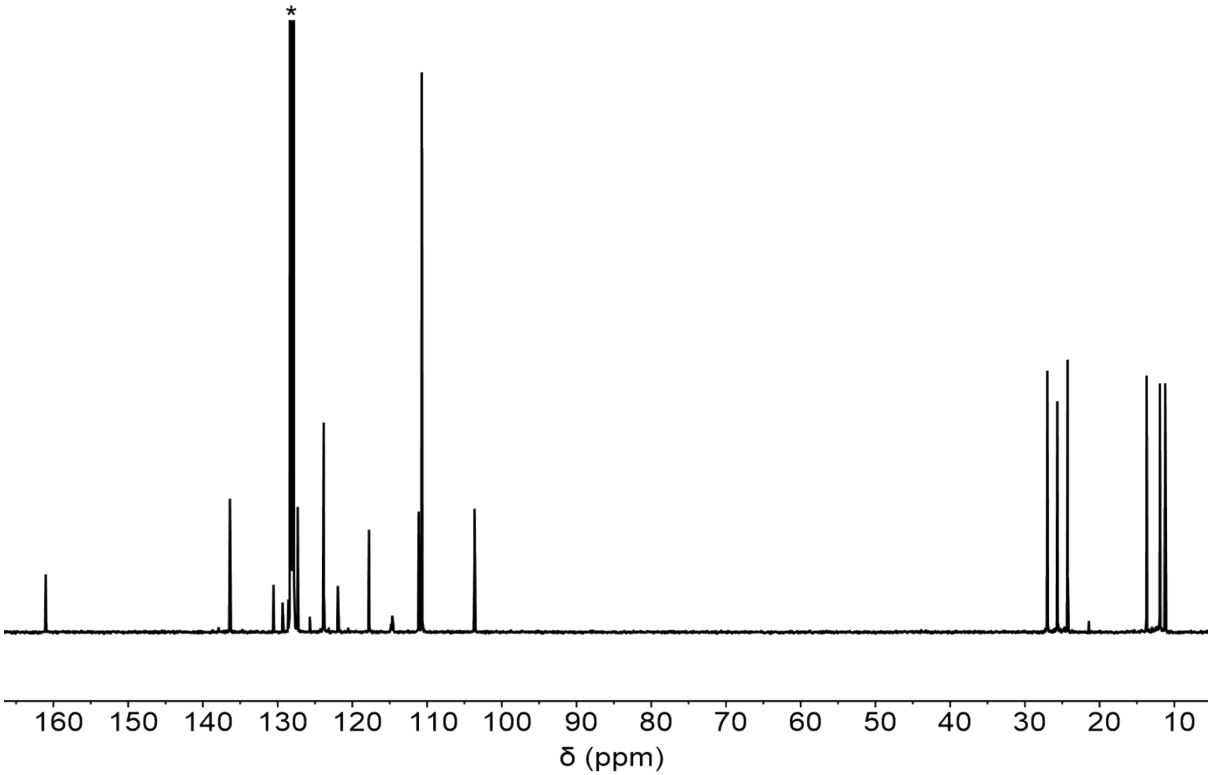

Fig. S16. $^{13}C\{^{1}H\}$ NMR spectrum (benzene-d_6 (*), 125 MHz, 298 K) of Pn*ZrCp(O-2,6-^{i}Pr-C_6H_3) (**9**).

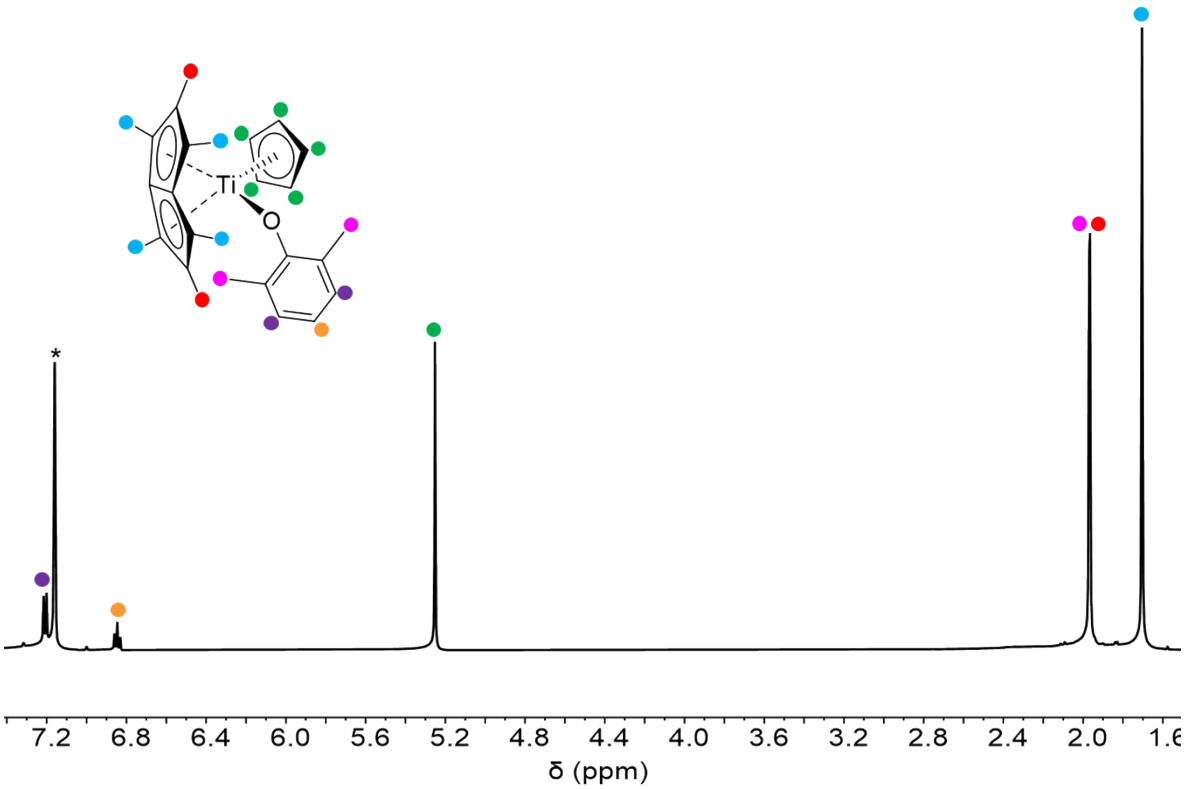

Fig. S17. ^{1}H NMR spectrum (benzene-d_6 (*), 500 MHz, 298 K) of Pn*TiCp(O-2,6-Me-C_6H_3) (**10**).

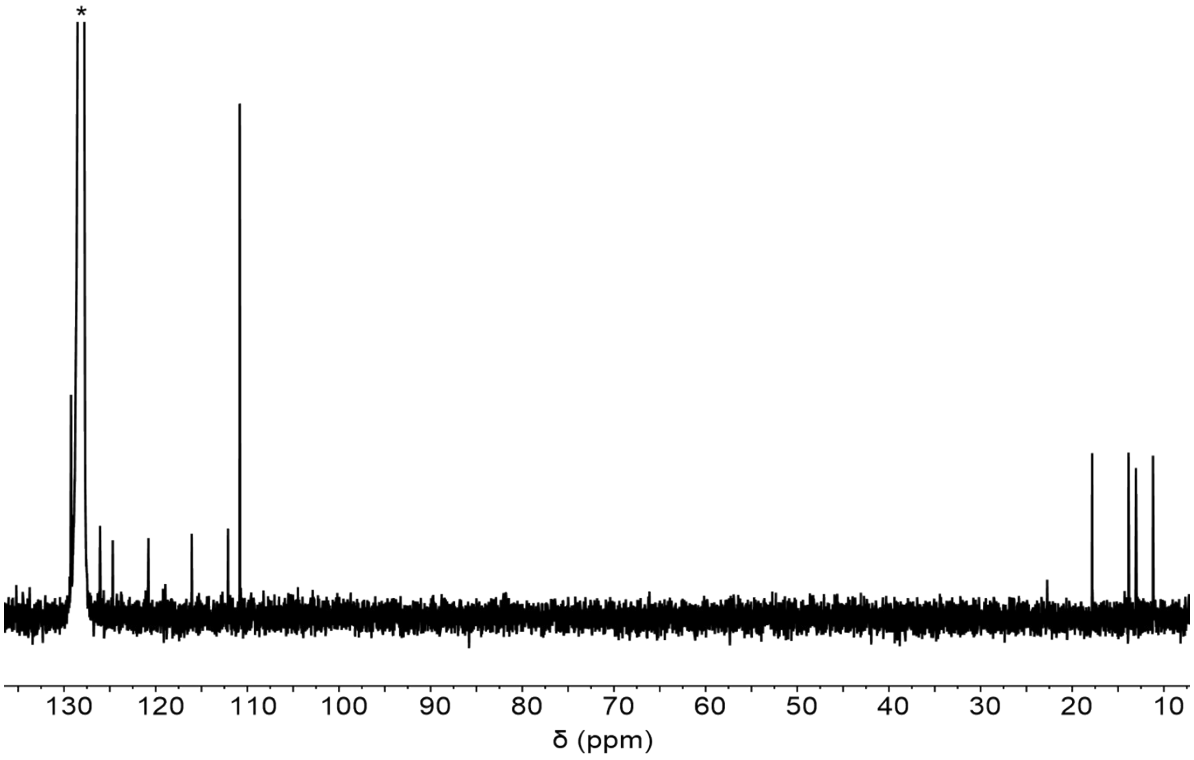

Fig. S18. $^{13}C\{^{1}H\}$ NMR spectrum (benzene-d_6 (*), 125 MHz, 298 K) of Pn*TiCp(O-2,6-Me-C_6H_3) (**10**).

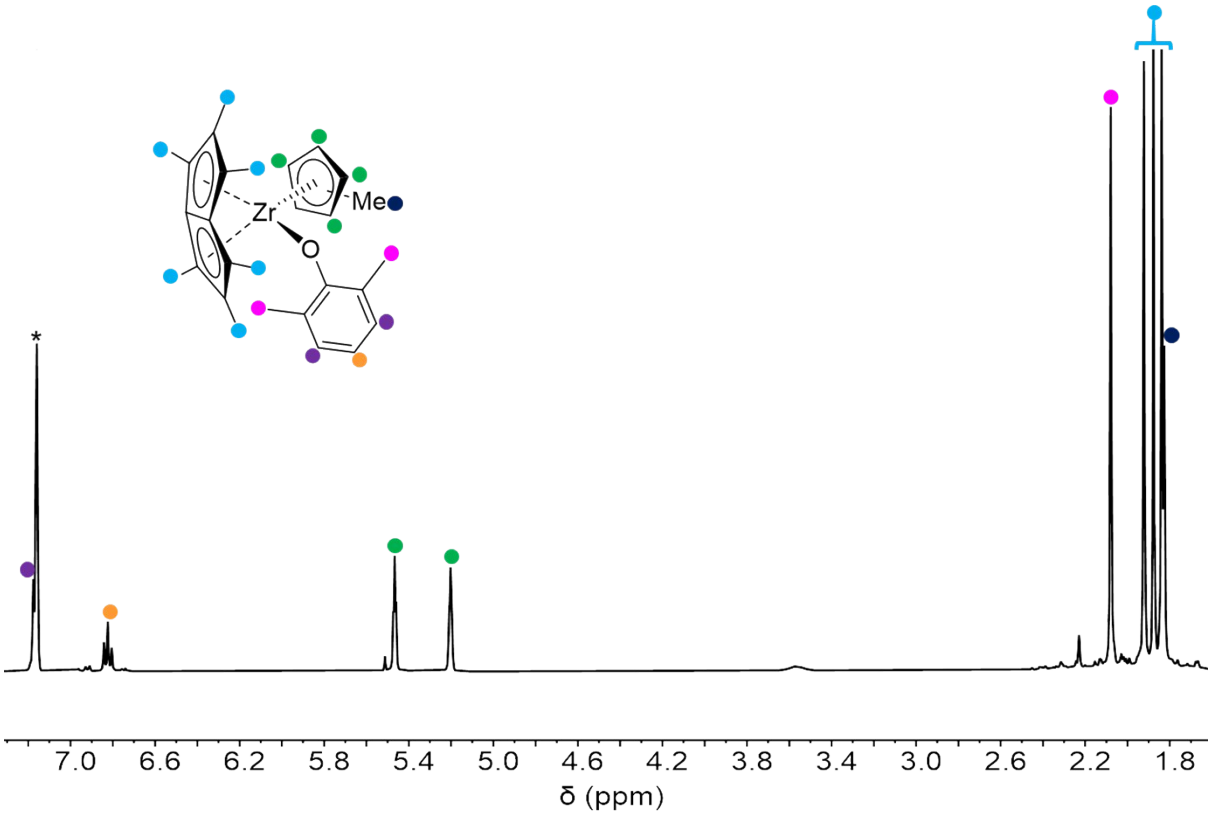

Fig. S19. ^{1}H NMR spectrum (benzene-d_6 (*), 400 MHz, 298 K) of Pn*ZrCp^{Me}(O-2,6-Me-C_6H_3) (**11**).

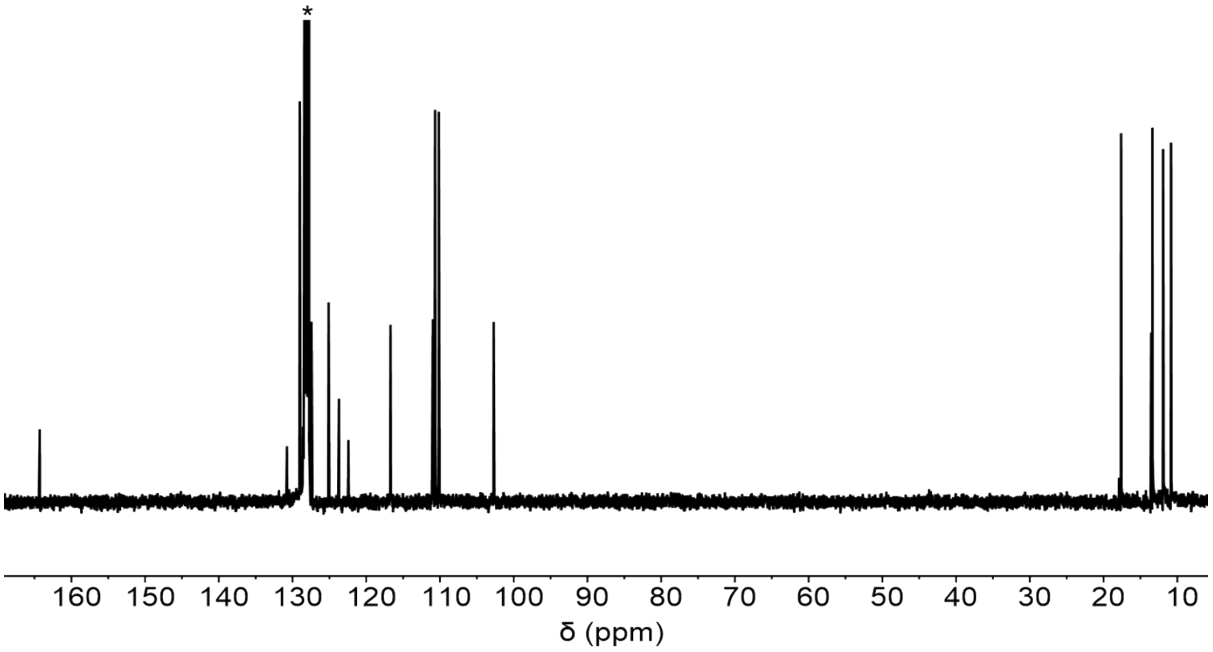

Fig. S20. $^{13}C\{^{1}H\}$ NMR spectrum (benzene-d_6 (*), 101 MHz, 298 K) of Pn*ZrCp^{Me}(O-2,6-Me-C_6H_3) (**11**).

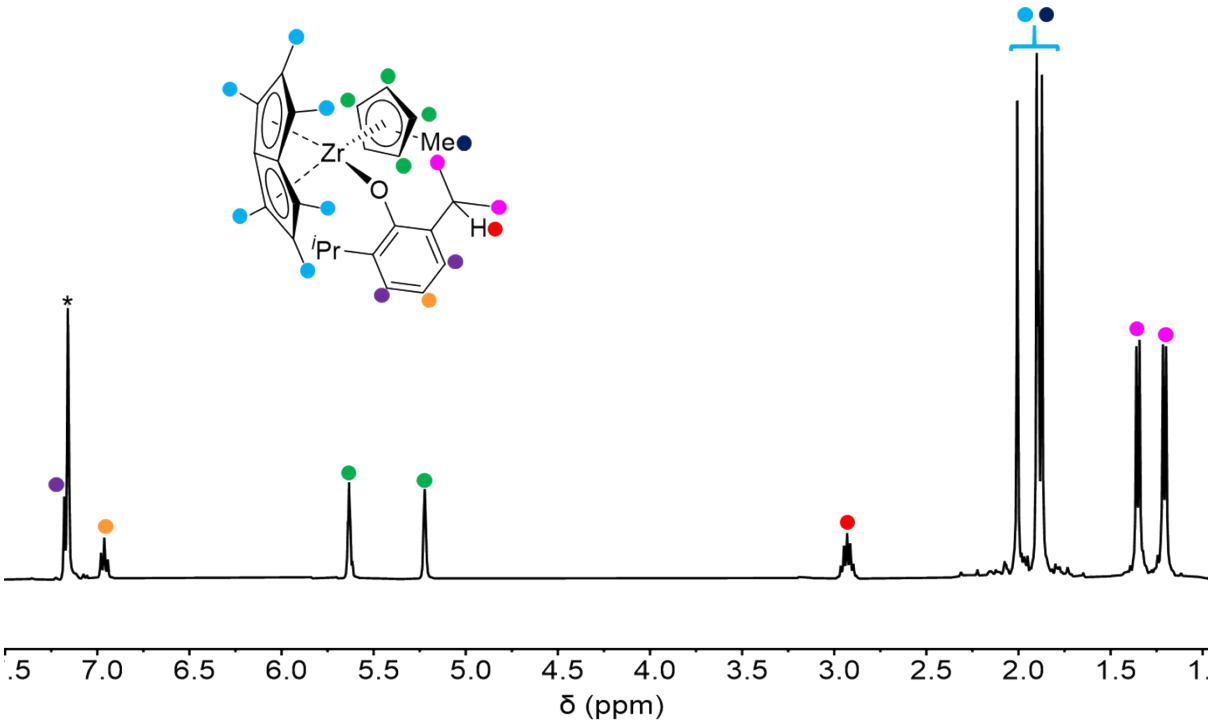

Fig. S21. ^{1}H NMR spectrum (benzene-d_6 (*), 400 MHz, 298 K) of Pn*ZrCp^{Me}(O-2,6-^{i}Pr-C_6H_3) (**12**).

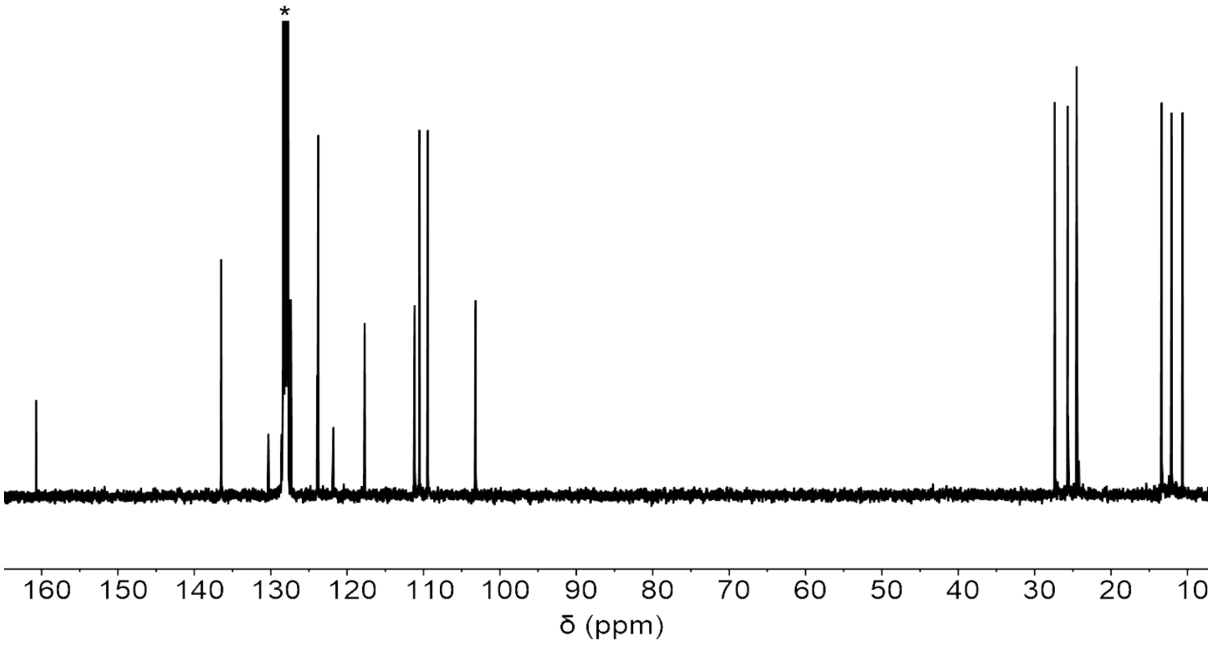

Fig. S22. $^{13}C\{^{1}H\}$ NMR spectrum (benzene-d_6 (*), 101 MHz, 298 K) of Pn*ZrCp^{Me}(O-2,6-^{i}Pr-C_6H_3) (**12**).

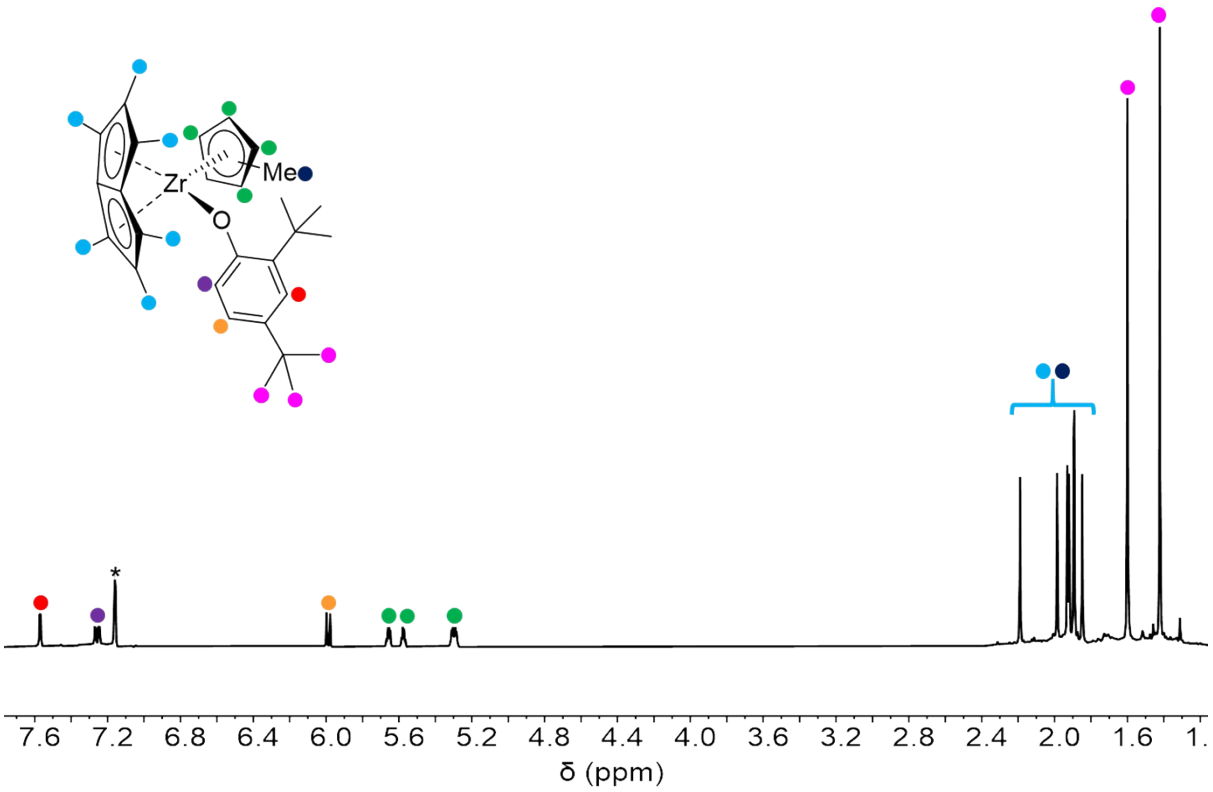

Fig. S23. ^{1}H NMR spectrum (benzene-d_6 (*), 400 MHz, 298 K) of Pn*ZrCp^{Me}(O-2,4-^{t}Bu-C_6H_3) (**13**).

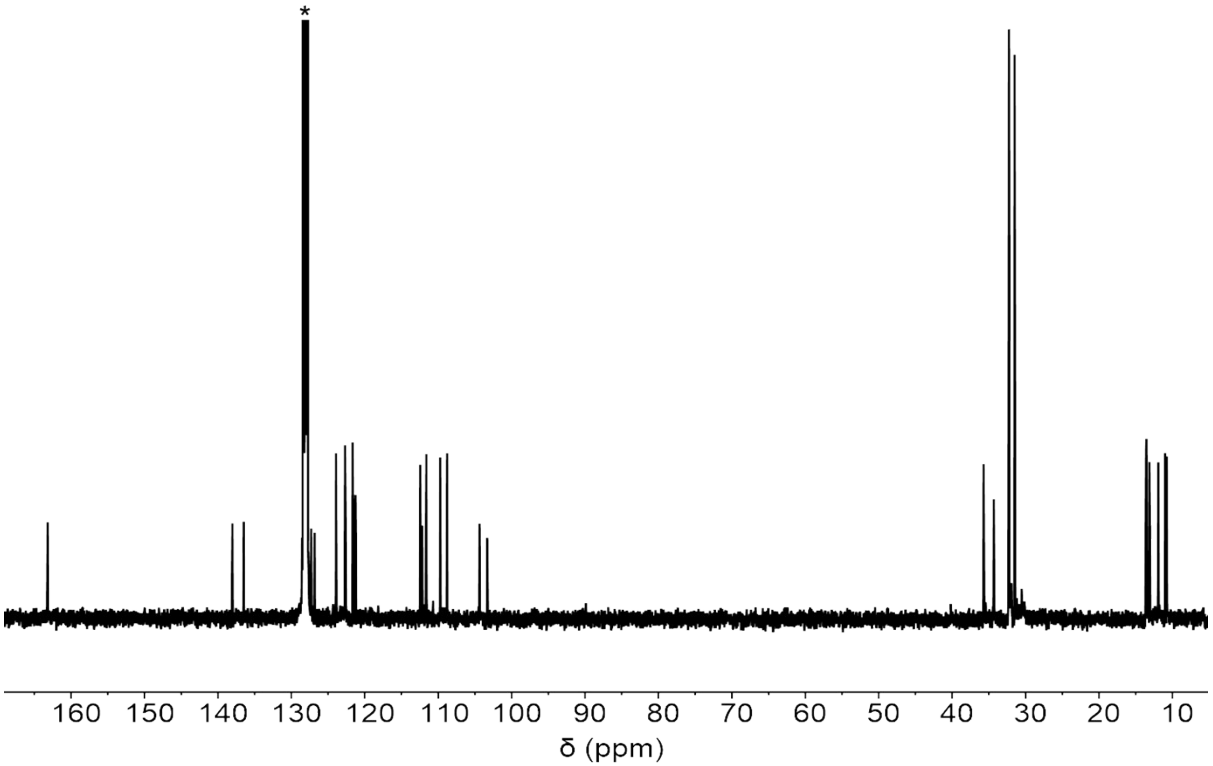

Fig. S24. $^{13}C\{^{1}H\}$ NMR spectrum (benzene-d_6 (*), 101 MHz, 298 K) of Pn*ZrCp^{Me}(O-2,4-^{t}Bu-C_6H_3) (**13**).

3. Additional crystallographic data

3.1 Crystallographic details

Crystals were mounted on MiTeGen MicroMounts using perfluoropolyether oil and rapidly transferred to a goniometer head on a diffractometer fitted with an Oxford Cryosystems Cryostream open-flow nitrogen cooling device.[8] Data collections were carried out at 150 K using an Oxford Diffraction Supernova diffractometer using mirror-monochromated Cu *Kα* radiation (λ = 1.54178 Å) and the data was processed using CrysalisPro.[9] The structures were solved using direct methods (SIR-92[10a] or SHELXS[10b,10c]) or a charge flipping algorithm (SUPERFLIP)[11] and refined by full-matrix least-squares procedures using the Win-GX software suite.[12]

An Enraf-Nonius Kappa CCD diffractometer using graphite monochromated Mo Kα radiation (λ = 0.71073 Å) was also used. Raw frame data were reduced using the DENZO-SMN package,[13] and corrected for absorption using SORTAV.[14] Intensity data were collected using a multi-scan method with SCALEPACK (within DENZO-SMN).

Compound **2** was refined as an inversion twin and compound **12** was refined as a two-component with the HKLF 5 method.

_vrf_PLAT910_091ZRT15
;
PROBLEM: Missing # of FCF Reflection(s) Below Theta(Min) 55
RESPONSE: 55 low-order reflections have been Omitted from the final least-squares refinement.

3.2. Experimental crystallographic data

Table S1. Selected experimental crystallographic data for Pn*Zr(O-2,6-Me-C_6H_3)$_2$ (**2**), Pn*Zr(O-2,6-^{i}Pr-C_6H_3)$_2$ (**3**), Pn*ZrCl(O-2,6-^{t}Bu-4-Me-C_6H_2) (**6**), and Pn*ZrCp^{Me}(O-2,6-^{i}Pr-C_6H_3) (**12**).

Complex	**Pn*Zr(O-2,6-Me-C_6H_3)$_2$**	**Pn*Zr(O-2,6-^{i}Pr-C_6H_3)$_2$**	**Pn*ZrCl(O-2,6-^{t}Bu-4-Me-C_6H_2)**	**Pn*ZrCp^{Me}(O-2,6-^{i}Pr-C_6H_3)**
		Crystal Data		
M_r	519.81	632.06	532.29	533.87
Crystal system	Monoclinic	Monoclinic	Monoclinic	Triclinic
Space group	$P2_1/n$	$P2_1/n$	$P2_1/n$	$P\bar{1}$
Temperature (K)	150	150	150	150
a (Å)	19.0444(3)	15.5176(2)	16.11460(10)	8.9476(2)
b (Å)	9.80080(10)	10.4812(10)	9.97050(10)	10.3488(3)
c (Å)	14.1408(2)	21.7454(2)	16.57600(10)	16.0319(4)
α (°)	90	90	90	92.631(2)
β (°)	93.3230(10)	106.515(1)	90.6800(10)	92.145(2)
γ (°)	90	90	90	115.499(2)
V (Å^3)	2634.95(6)	3390.83(6)	2663.09(4)	1335.79(6)
Z	4	4	4	2
Radiation type	Cu $K\alpha$	Cu $K\alpha$	Cu $K\alpha$	Cu $K\alpha$
μ (mm^{-1})	3.59	0.35	4.43	3.52
Crystal size (mm)	0.20 × 0.10 × 0.09	0.40 × 0.30 × 0.10	0.20 × 0.18 × 0.15	0.12 × 0.10 × 0.08

Data Collection				
Diffractometer	SuperNova, Dual, Cu at zero, Atlas	Nonius KappaCCD HKL scale pack (Otwinowski & Minoe 1997), Mo	SuperNova, Dual, Cu at zero, Atlas	SuperNova, Dual, Cu at zero, Atlas
Absorption correction	Multi-scan *CrysAlis*Pro 1.171.38.43b (Rigaku Oxford Diffraction, 2015) Empirical absorption correction using spherical harmonics, implemented in SCALE3 ABSPACK scaling algorithm.	Multi-scan from symmetry-related measurements using Sortav (Blessing 1995)	Multi-scan *CrysAlis*Pro 1.171.38.43b (Rigaku Oxford Diffraction, 2015). Empirical absorption correction using spherical harmonics, implemented in SCALE3 ABSPACK scaling algorithm.	Multi-scan *CrysAlis*Pro 1.171.38.41 (Rigaku Oxford Diffraction, 2015). Empirical absorption correction using spherical harmonics, implemented in SCALE3 ABSPACK scaling algorithm.
T_{min}, T_{max}		0.911, 1.000	0.679, 1.000	0.870,1.000
No. of measured, independent and observed [$I > 2\sigma(I)$] reflections	26430, 5473, 4492	15861, 8330, 6699	28211, 5554, 5190	9810, 9810, 9150
R_{int}	0.024	0.026	0.023	-
Refinement				
$R[F^2 > 2\sigma(F^2)]$, $wR(F^2)$, S	0.0292, 0.0802 1.034	0.034, 0.092, 1.051	0.0216, 0.0600, 1.073	0.034, 0.091, 1.10
No. of reflections	547	8330	5554	9810
No. of parameters	558	384	302	319
No. of restraints	23	0	0	0
$(\Delta/\sigma)_{max}$	0.001	0.002	0.001	0.001
$\Delta\rho_{max}$, $\Delta\rho_{min}$ (e Å^{-3})	0.35, −0.63	0.60, −0.62	0.33, −0.46	0.92, −0.70

Table S2. Selected experimental crystallographic data for Pn*ZrCl(O-2,6-Me-C_6H_3), Pn*ZrCl(O-2,6-^{t}Bu-C_6H_3).tmeda and [Pn*Zr(O-4-OMe-C_6H_4)$_2$]$_2$ (**4'**).

Complex	Pn*ZrCl(O-2,6-Me-C_6H_3)	Pn*ZrCl(O-2,6-^{t}Bu-C_6H_3).tmeda	[Pn*Zr(O-4-OMe-C_6H_4)$_2$]$_2$
Crystal Data			
M_r	434.10	676.86	523.75
Crystal system	Triclinic	Triclinic	Triclinic
Space group	$P\bar{1}$	$P\bar{1}$	$P\bar{1}$
Temperature (K)	150	150	150
a (Å)	10.6046(6)	10.5832(2)	9.8414(5)
b (Å)	12.2355(5)	12.6630(3)	11.4573(5)
c (Å)	17.2888(8)	15.2987(3)	11.9108(5)
α (°)	75.850(4)	72.614(2)	114.746(4)
β (°)	87.114(4)	70.176(2)	92.331(4)
γ (°)	67.084(4)	67.102(2)	98.792(4)
V (Å^3)	2001.00(18)	1743.52(7)	1197.13(10)
Z	4	2	2
Radiation type	Cu $K\alpha$	Cu $K\alpha$	Cu $K\alpha$
μ (mm^{-1})	5.77	4.19	4.02
Crystal size (mm)	0.16 × 0.10 × 0.05	0.18 × 0.13 × 0.10	0.17 × 0.08 × 0.04
Data Collection			
Diffractometer	SuperNova, Dual, Cu at zero, Atlas	SuperNova, Dual, Cu at zero, Atlas	SuperNova, Dual, Cu at zero, Atlas
Absorption correction	Gaussian	Multi-scan	Gaussian

	*CrysAlis*Pro 1.171.38.43b (Rigaku Oxford Diffraction, 2015). Numerical absorption correction based on gaussian integration over a multifaceted crystal model. Empirical absorption correction using spherical harmonics, implemented in SCALE3 ABSPACK scaling algorithm.	*CrysAlis*Pro, Agilent Technologies, Version 1.171.35.2. Empirical absorption correction using spherical harmonics, implemented in SCALE3 ABSPACK scaling algorithm.	*CrysAlis*Pro 1.171.38.43b (Rigaku Oxford Diffraction, 2015). Numerical absorption correction based on gaussian integration over a multifaceted crystal model. Empirical absorption correction using spherical harmonics, implemented in SCALE3 ABSPACK scaling algorithm.
T_{min}, T_{max}	0.475, 1.000	0.723,1.000	0.622, 0.972
No. of measured, independent and observed [$I > 2\sigma(I)$] reflections	20196, 8271, 7315	35966, 7230, 7083	11326, 4939, 4685
R_{int}	0.028	0.016	0.027
Refinement			
$R[F^2 > 2\sigma(F^2)]$, $wR(F^2)$, S	0.058, 0.062, 1.056	0.021, 0.054, 1.035	0.0224, 0.0564, 1.045
No. of reflections	8271	7230	4939
No. of parameters	467	404	306
No. of restraints	0	25	0
$(\Delta/\sigma)_{max}$	0.003	0.002	0.000
$\Delta\rho_{max}$, $\Delta\rho_{min}$ (e Å^{-3})	0.37, −0.47	0.45, −0.44	0.27, −0.36

Computer programs: CrysAlisPro 1.171.39.46 (Rigaku OD, 2018), CrysAlisPro 1.171.38.41 (Rigaku OD, 2015), SUPERFLIP Palatinus, L.; Chapuis, G. J. Appl. Cryst. 2007, 40, 786-790., *SIR92* Altomare, A.; Cascarano, G.; Giacovazzo, C.; Guagliardi, A. J. Appl. Cryst. 1994, 27, 435., SUPERFLIP. Palatinus, L.; Chapuis, G. J. Appl. Cryst. 2007, 40, 786-790., *SHELXL2014* (Sheldrick, 2014), *ORTEP-3 for Windows*. Farrugia, L. J. J. Appl. Cryst. 1997, 30, 565.

4. Polymerisation data

4.1 Polymerisation graphs

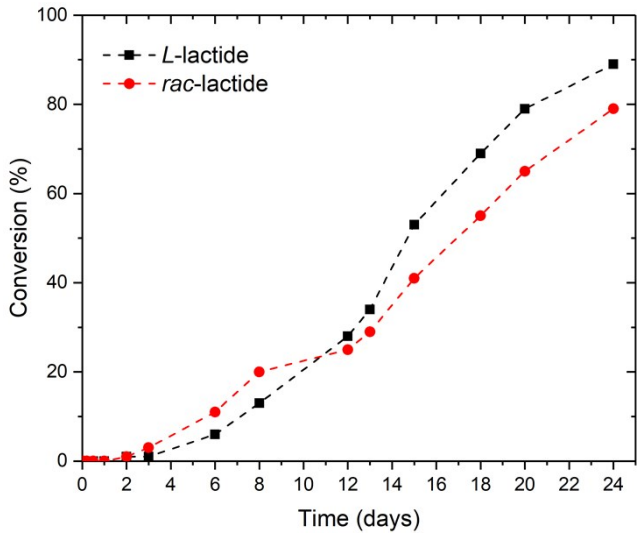

Fig. S25. Percentage conversion to PLA as a function of time of polymerisation for the ROP of *L*- (black square) and *rac*-lactide (red circle) using Pn*TiCp(O-2,6-Me-C_6H_3). Polymerisation conditions: 80 °C, $[LA]_0/[M]_0 = 50$, $[LA]_0 = 0.5$ M and benzene-d_6.

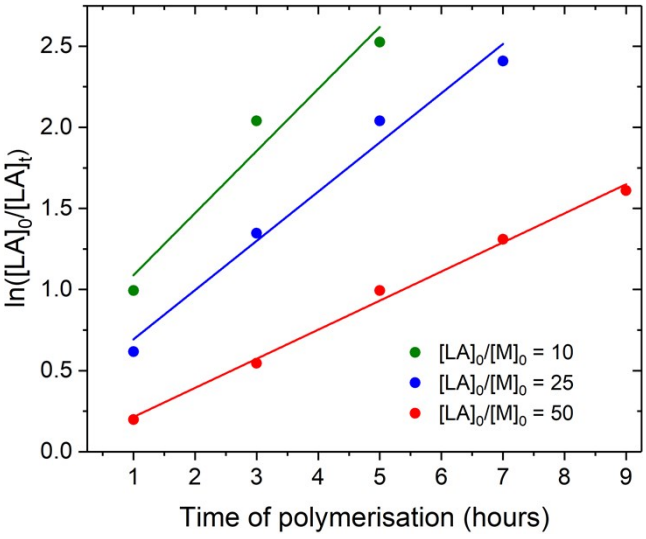

Fig. S26. $\ln([LA]_0/[LA]_t)$ as a function of time of polymerisation for the ROP of *rac*-lactide using Pn*Zr(O-2,6-^{i}Pr-$C_6H_3)_2$ (**3**) with $[LA]_0/[M]_0 = 10$ (green, $k_{obs} = 0.38 \pm 0.08$ h^{-1}), $[LA]_0/[M]_0 = 25$ (blue, $k_{obs} = 0.30 \pm 0.03$ h^{-1}) and $[LA]_0/[M]_0 = 50$ (red, $k_{obs} = 0.18 \pm 0.01$ h^{-1}). Polymerisation conditions: 80 °C, $[LA]_0 = 0.5$ M and benzene-d_6.

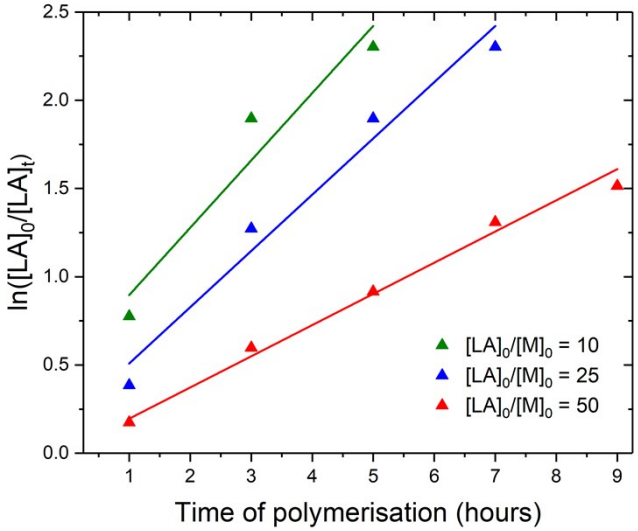

Fig. S27. $\ln([LA]_0/[LA]_t)$ as a function of time of polymerisation for the ROP of *rac*-lactide using Pn*ZrCl(O-2,6-^{t}Bu-4-Me-C_6H_2) (**6**) with $[LA]_0/[M]_0 = 10$ (green, $k_{obs} = 0.38 \pm 0.10$ h^{-1}), $[LA]_0/[M]_0 = 25$ (blue, $k_{obs} = 0.32 \pm 0.04$ h^{-1}) and $[LA]_0/[M]_0 = 50$ (red, $k_{obs} = 0.18 \pm 0.01$ $^{-1}$). Polymerisation conditions: 80 °C, $[LA]_0 = 0.5$ M and benzene-d_6.

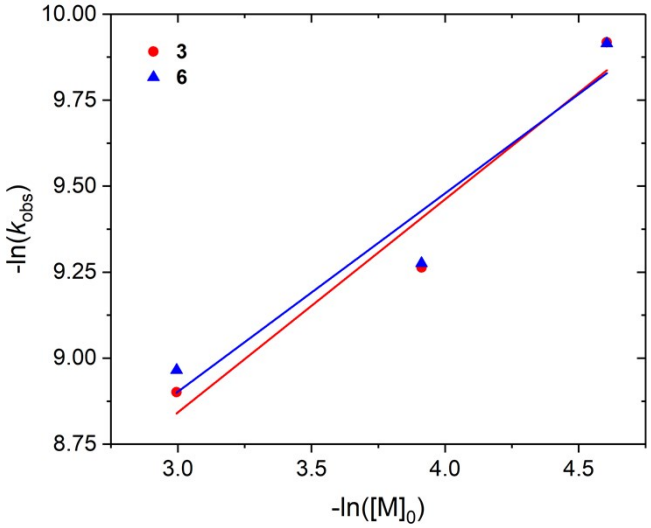

Fig. S28. $-\ln(k_{app})$ as a function of $-\ln([M]_0)$ for the polymerisation of *rac*-lactide using Pn*Zr(O-2,6-^{i}Pr-C_6H_3)$_2$ (**3**) (red circle, slope = 0.62 ± 0.15 with $R^2 = 0.941$) and Pn*ZrCl(O-2,6-^{t}Bu-4-Me-C_6H_2) (**6**) (blue triangle, slope = 0.58 ± 0.16 with $R^2 = 0.925$). Polymerisation conditions: 80 °C, $[LA]_0 = 0.5$ M and benzene-d_6.

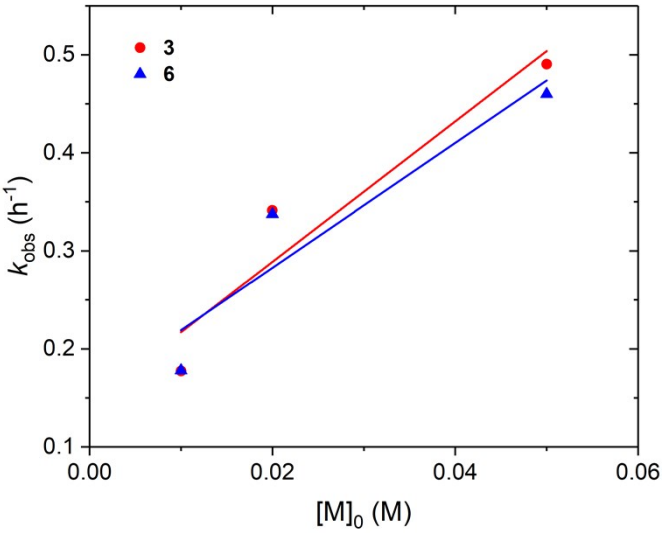

Fig. S29. k_{obs} as a function of $[M]_0$ for the polymerisation of *rac*-lactide using Pn*Zr(O-2,6-^{i}Pr-$C_6H_3)_2$ (**3**) (red circle, slope = 7.17 ± 2.29 h^{-1} M^{-1} with R^2 = 0.908) and Pn*ZrCl(O-2,6-^{t}Bu-4-Me-C_6H_2) (**6**) (blue triangle, slope = 6.37 ± 2.37 h^{-1} M^{-1} with R^2 = 0.879). Polymerisation conditions: 80 °C, $[LA]_0$ = 0.5 M and benzene-d_6.

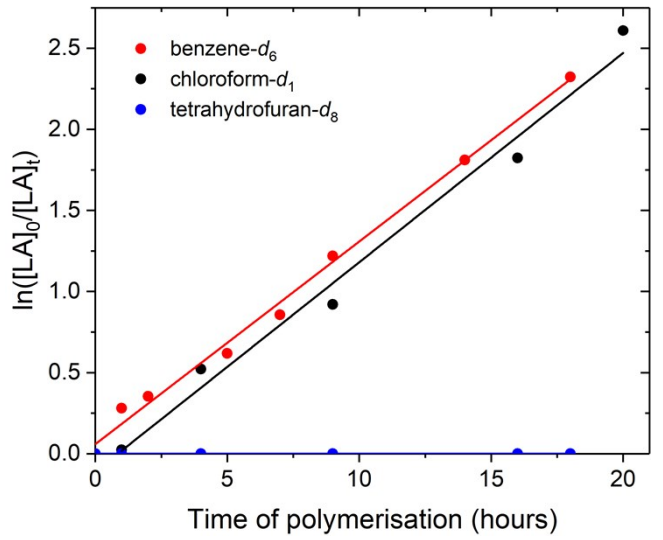

Fig. S30. $\ln([LA]_0/[LA]_t)$ as a function of time of polymerisation for the ROP of *rac*-lactide using Pn*Zr(O-2,6-^{i}Pr-$C_6H_3)_2$ (**3**) in benzene-d_6 (red circle, k_{obs} = 0.12 ± 0.01 h^{-1}), chloroform-d_1 (black circle, k_{obs} = 0.13 ± 0.01 h^{-1}) and tetrahydrofuran-d_8 (blue circle, k_{obs} = 0 h^{-1}). Polymerisation conditions: 80 °C, $[LA]_0/[M]_0$ = 200 and $[LA]_0$ = 2.0 M.

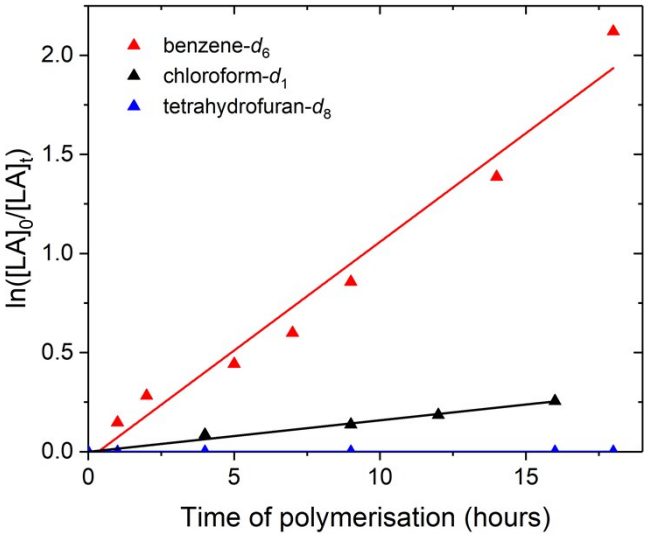

Fig. S31. ln([LA]$_0$/[LA]$_t$) as a function of time of polymerisation for the ROP of *rac*-lactide using Pn*ZrCl(O-2,4-^{t}Bu-C_6H_2) (**6**) in benzene-d_6 (red triangle, k_{obs} = 0.11 ± 0.01 h^{-1}), chloroform-d_1 (black triangle, k_{obs} = 0.01 ± 0.001 h^{-1}) and tetrahydrofuran-d_8 (blue triangle, k_{obs} = 0 h^{-1}). Polymerisation conditions: 80 °C, [LA]$_0$/[M]$_0$ = 200 and [LA]$_0$ = 2.0 M.

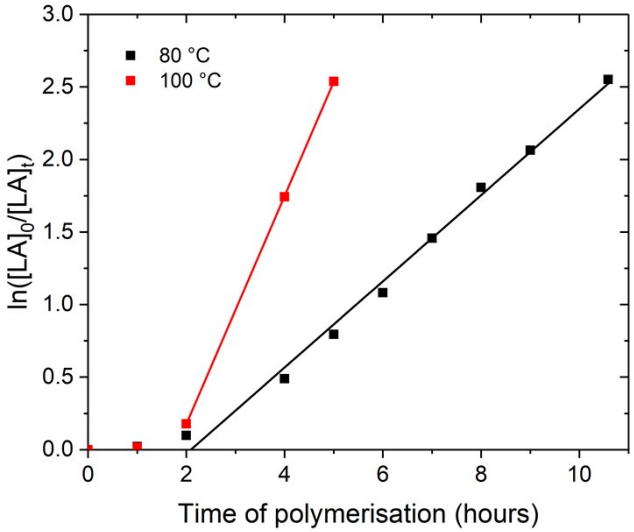

Fig. S32. ln([LA]$_0$/[LA]$_t$) as a function of time of polymerisation for the ROP of *L*-lactide using Pn*Zr(O-2,6-Me-C_6H_3)$_2$ (**2**) at 80 °C (black square, k_{obs} = 0.30 ± 0.01 h^{-1}) and 100 °C (red square, k_{obs} = 0.79 ± 0.01 h^{-1}). Polymerisation conditions: [LA]$_0$/[M]$_0$ = 50, [LA]$_0$ = 0.5 M and benzene-d_6.

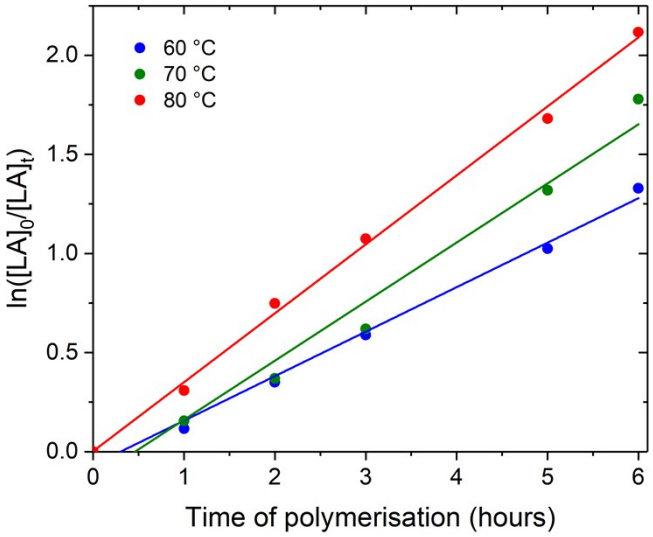

Fig. S33. $\ln([LA]_0/[LA]_t)$ as a function of time of polymerisation for the ROP of *L*-lactide using Pn*Zr(O-2,6-^{i}Pr-C_6H_3)$_2$ (**3**) at 60 °C (blue circle, k_{obs} = 0.22 ± 0.01 h^{-1}), 70 °C (green circle, k_{obs} = 0.30 ± 0.02 h^{-1}) and 80 °C (red circle, k_{obs} = 0.35 ± 0.01 h^{-1}). Polymerisation conditions: $[LA]_0/[M]_0$ = 50, $[LA]_0$ = 0.5 M and benzene-d_6.

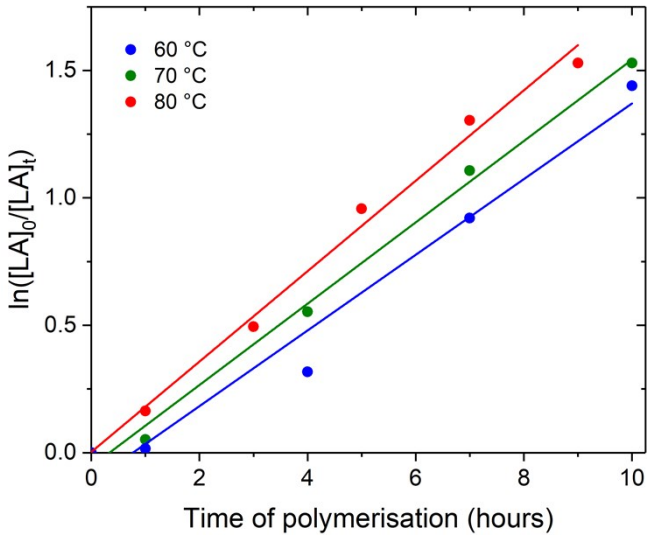

Fig. S34. $\ln([LA]_0/[LA]_t)$ as a function of time of polymerisation for the ROP of *rac*-lactide using Pn*Zr(O-2,6-^{i}Pr-C_6H_3)$_2$ (**3**) at 60 °C (blue circle, k_{obs} = 0.15 ± 0.01 h^{-1}), 70 °C (green circle, k_{obs} = 0.16 ± 0.01 h^{-1}) and 80 °C (red circle, k_{obs} = 0.18 ± 0.01 h^{-1}). Polymerisation conditions: $[LA]_0/[M]_0$ = 50, $[LA]_0$ = 0.5 M and benzene-d_6.

4.2 Polymerisation activities, conversions and molecular weights tables

Table S3. *L*-Lactide polymerisation using Pn*Zr(O-2,6-Me-C_6H_3)$_2$ (**2**), Pn*Zr(O-2,6-^{i}Pr-C_6H_3)$_2$ (**3**), Pn*ZrCl(O-2,6-^{t}Bu-4-Me-C_6H_2) (**6**), Pn*ZrCp(O^{t}Bu) (**7**), Pn*ZrCp(O-2,6-iPr-C_6H_3) (**9**) and Pn*ZrCp^{Me}(O-2,6-^{i}Pr-C_6H_3) (**12**).

Initiator	$[LA]_0/[M]_0$	$[LA]_0$ (M)	Temp. (°C)	Solvent	Time[a] (h)	Conversion[b] (%)	k_{obs} (h^{-1})	R^2	M_n (calcd)[c] (g mol^{-1})	M_n (GPC)[d] (g mol^{-1})	M_w/M_n[d]
2	50	0.5	80	benzene-d_6	10.6	92	0.30 ± 0.01	0.992	-	-	-
3	50	0.5	80	benzene-d_6	6	88	0.35 ± 0.01	0.997	6520	17398	1.62
7	50	0.5	80	benzene-d_6	30	92	0.09 ± 0.01	0.966	-	-	-
9	50	0.5	80	benzene-d_6	50	79	0.03 ± 0.001	0.998	-	-	-
12	50	0.5	80	benzene-d_6	164	85	0.01 ± 0.001	0.998	-	-	-
2	200	2.0	80	benzene-d_6	21	98	0.30 ± 0.03	0.964	28374	30709	1.37
3	200	2.0	80	benzene-d_6	28	98	0.32 ± 0.04	0.957	28430	31327	1.28
6	200	2.0	80	benzene-d_6	24	36	0.02 ± 0.001	0.981	10598	12950	1.45
3	50	0.5	60	benzene-d_6	6	74	0.22 ± 0.01	0.992	5511	14282	1.21
3	50	0.5	70	benzene-d_6	6	83	0.30 ± 0.02	0.974	6160	14346	1.62
2	50	0.5	100	benzene-d_6	6	94	0.79 ± 0.01	0.999	-	-	-

(a) Time polymerisation quenched; (b) Measured by ^{1}H NMR spectroscopic analysis; (c) M_n (calcd) = (M_{LA} × $[LA]_0/[M]_0$ × (conv.(%)/100) + $M_{end\ group}$; (d) Determined by GPC in chloroform at 30 °C against polystyrene standards (M_n values are corrected by a factor of 0.58).[7]

Table S4. *rac*-Lactide polymerisation using Pn*Zr(O-2,6-Me-C_6H_3)$_2$ (**2**), Pn*Zr(O-2,6-^{i}Pr-C_6H_3)$_2$ (**3**), Pn*ZrCl(O-2,6-^{t}Bu-4-Me-C_6H_2) (**6**) and Pn*ZrCp(O^{t}Bu) (**7**).

Initiator	$[LA]_0/[M]_0$	$[LA]_0$ (M)	Temp. (°C)	Solvent	Time[a] (h)	Conversion[b] (%)	k_{obs} (h^{-1})	R^2	M_n (calcd)[c] (g mol^{-1})	M_n (GPC)[d] (g mol^{-1})	M_w/M_n[d]
3	50	0.5	80	benzene-d_6	9	78	0.18 ± 0.01	0.992	5800	9930	1.57
6	50	0.5	80	benzene-d_6	9	79	0.18 ± 0.01	0.995	5914	6617	1.56
7	50	0.5	80	benzene-d_6	30	87	0.04 ± 0.001	0.999	-	-	-
2	200	2.0	80	benzene-d_6	21	98	0.21 ± 0.02	0.977	28374	25275	1.23
3	200	2.0	80	benzene-d_6	30	97	0.12 ± 0.01	0.994	28141	25509	1.14
5	200	2.0	80	benzene-d_6	24	95	0.11 ± 0.01	0.974	27607	26747	1.38
3	50	0.5	60	benzene-d_6	10	76	0.15 ± 0.01	0.972	5656	7999	1.27
3	50	0.5	70	benzene-d_6	10	78	0.16 ± 0.01	0.995	5842	9800	1.51
3	25	0.5	80	benzene-d_6	7	91	0.34 ± 0.03	0.972	3457	4337	1.86
3	10	0.5	80	benzene-d_6	5	92	0.49 ± 0.09	0.933	-	-	-
6	25	0.5	80	benzene-d_6	7	90	0.34 ± 0.03	0.980	3464	3673	1.28
6	10	0.5	80	benzene-d_6	5	90	0.46 ± 0.08	0.942	-	-	-
3	200	2	80	chloroform-d_1	20	93	0.13 ± 0.01	0.984	26988	9930	1.57
3	200	2	80	tetrahydrofuran-d_8	24	0	0	-	-	-	-
5	200	2	80	chloroform-d_1	16	23	0.01 ± 0.001	0.984	6851	4337	1.86
6	200	2	80	tetrahydrofuran-d_8	24	0	0	-	-	-	-

(a) Time polymerisation quenched; (b) Measured by ^{1}H NMR spectroscopic analysis; (c) M_n (calcd) = ($M_{LA} \times [LA]_0/[M]_0 \times$ (conv.(%)/100) + $M_{end\ group}$; (d) Determined by GPC in chloroform at 30 °C against polystyrene standards (M_n values are corrected by a factor of 0.58).[7]

Table S5. *L*-Lactide polymerisation using Pn*Zr(O-2,6-Me-C_6H_3) (**2**) at 80 °C with $[LA]_0/[M]_0 = 50$ and $[LA]_0 = 0.5$ M in benzene-d_6.

Time (h)	Conversion (%)	$[LA]_0/[LA]_t$
0	0	0
1	2	0.02
2	9	0.09
4	39	0.49
5	55	0.79
6	66	1.08
7	77	1.46
8	84	1.81
9	87	2.06
10.6	92	2.55

Table S6. *L*-Lactide polymerisation using Pn*Zr(O-2,6-^{i}Pr-C_6H_3)$_2$ (**3**) at 80 °C with $[LA]_0/[M]_0 = 50$ and $[LA]_0 = 0.5$ M in benzene-d_6.

Time (h)	Conversion (%)	$[LA]_0/[LA]_t$
0	0	0
1	27	0.31
2	53	0.75
3	66	1.07
5	81	1.68
6	88	2.12

Table S7. *L*-Lactide polymerisation using Pn*ZrCp(O^{t}Bu) (**7**) at 80 °C with $[LA]_0/[M]_0 = 50$ and $[LA]_0 = 0.5$ M in benzene-d_6.

Time (h)	Conversion (%)	$[LA]_0/[LA]_t$
0	0	0
1	1	0.01
3	6	0.04
18.5	65	1.05
28.5	89	2.23
30	92	2.56

Table S8. *L*-Lactide polymerisation using Pn*ZrCp(O-2,6-^{i}Pr-C_6H_3) (**9**) at 80 °C with $[LA]_0/[M]_0 = 50$ and $[LA]_0 = 0.5$ M in benzene-d_6.

Time (h)	Conversion (%)	$[LA]_0/[LA]_t$
0	0	0
1	1	0.01
3	2	0.02
18.5	37	0.47
42	72	1.28
50	79	1.57

Table S9. *L*-Lactide polymerisation using Pn*TiCp(O-2,6-Me-C_6H_3) (**10**) at 80 °C with $[LA]_0/[M]_0 = 50$ and $[LA]_0 = 0.5$ M in benzene-d_6.

Time (h)	Conversion (%)
0.5	0
1	0
2	1
3	1
6	6
8	13
12	28
13	34
15	53
18	69
20	79
24	89

Table S10. *L*-Lactide polymerisation using Pn*ZrCp^{Me}(O-2,6-^{i}Pr-C_6H_3) (**12**) at 80 °C with $[LA]_0/[M]_0 = 50$ and $[LA]_0 = 0.5$ M in benzene-d_6.

Time (h)	Conversion (%)	$[LA]_0/[LA]_t$
0	0	0
16	4	0.04
32	12	0.12
54	26	0.30
77	42	0.54
100	60	0.91
164	85	1.92

Table S11. *L*-Lactide polymerisation using Pn*Zr(O-2,6-Me-C_6H_3)$_2$ (**2**) at 80 °C with $[LA]_0/[M]_0 = 200$ and $[LA]_0 = 2.0$ M in benzene-d_6.

Time (h)	Conversion (%)	$[LA]_0/[LA]_t$
0	0	0
3	11	0.12
5	34	0.42
7	64	1.02
9	84	1.82
14	97	3.51
21	98	3.76

Table S12. *L*-Lactide polymerisation using Pn*Zr(O-2,6-^{i}Pr-C_6H_3)$_2$ (**3**) at 80 °C with $[LA]_0/[M]_0 = 200$ and $[LA]_0 = 2.0$ M in benzene-d_6.

Time (h)	Conversion (%)	$[LA]_0/[LA]_t$
0	0	0
1	25	0.29
2	44	0.58
5	70	1.20
7	91	2.37
9	95	2.97
18	95	2.99
21	96	3.31
24	97	3.63
28	98	3.79

Table S13. *L*-Lactide polymerisation using Pn*ZrCl(O-2,6-^{t}Bu-4-Me-C_6H_2) (**6**) at 80 °C with $[LA]_0/[M]_0 = 200$ and $[LA]_0 = 2.0$ M in benzene-d_6.

Time (h)	Conversion (%)	$[LA]_0/[LA]_t$
0	0	0
1	2	0.02
2	4	0.04
5	6	0.06
7	12	0.13
9	20	0.22
14	25	0.29
18	29	0.34
21	32	0.39
24	36	0.45

Table S14. *L*-Lactide polymerisation using Pn*Zr(O-2,6-^{i}Pr-C_6H_3)$_2$ (**3**) at 60 °C with $[LA]_0/[M]_0 = 50$ and $[LA]_0 = 0.5$ M in benzene-d_6.

Time (h)	Conversion (%)	$[LA]_0/[LA]_t$
0	0	0
1	11	0.12
2	30	0.35
3	44	0.59
5	64	1.02
6	74	1.33

Table S15. *L*-Lactide polymerisation using Pn*Zr(O-2,6-^{i}Pr-C_6H_3)$_2$ (**3**) at 70 °C with $[LA]_0/[M]_0 = 50$ and $[LA]_0 = 0.5$ M in benzene-d_6.

Time (h)	Conversion (%)	$[LA]_0/[LA]_t$
0	0	0
1	14	0.16
2	31	0.37
3	46	0.62
5	73	1.32
6	83	1.78

Table S16. *L*-Lactide polymerisation using Pn*Zr(O-2,6-Me-C_6H_3) (**2**) at 100 °C with $[LA]_0/[M]_0 = 50$ and $[LA]_0 = 0.5$ M in benzene-d_6.

Time (h)	Conversion (%)	$[LA]_0/[LA]_t$
0	0	0
1	2	0.02
2	16	0.16
4	83	0.83
5	92	0.92
6	94	0.94

Table S17. *rac*-Lactide polymerisation using Pn*Zr(O-2,6-^{i}Pr-$C_6H_3)_2$ (**3**) at 80 °C with $[LA]_0/[M]_0 = 50$ and $[LA]_0 = 0.5$ M in benzene-d_6.

Time (h)	Conversion (%)	$[LA]_0/[LA]_t$
0	0	0
1	15	0.16
3	39	0.49
5	62	0.96
7	73	1.30
9	78	1.53

Table S18. *rac*-Lactide polymerisation using Pn*ZrCl(O-2,6-^{t}Bu-4-Me-C_6H_2) (**6**) at 80 °C with $[LA]_0/[M]_0 = 50$ and $[LA]_0 = 0.5$ M in benzene-d_6.

Time (h)	Conversion (%)	$[LA]_0/[LA]_t$
0	0	0
1	14	0.15
3	45	0.59
5	59	0.90
7	73	1.31
9	79	1.55

Table S19. *rac*-Lactide polymerisation using Pn*ZrCp(O^{t}Bu) (**7**) at 80 °C with $[LA]_0/[M]_0 = 50$ and $[LA]_0 = 0.5$ M in benzene-d_6.

Time (h)	Conversion (%)	$[LA]_0/[LA]_t$
0	0	0
1	2	0.02
3	9	0.10
19	55	0.81
29	86	1.80
30	87	2.07

Table S20. *rac*-Lactide polymerisation using Pn*TiCp(O-2,6-Me-C_6H_3) (**10**) at 80 °C with $[LA]_0/[M]_0 = 50$ and $[LA]_0 = 0.5$ M in benzene-d_6.

Time (h)	Conversion (%)
0.5	0
1	0
2	1
3	3
6	11
8	20
12	25
13	29
15	41
18	55
20	65
24	79

Table S21. *rac*-Lactide polymerisation using Pn*Zr(O-2,6-Me-C_6H_3)$_2$ (**2**) at 80 °C with $[LA]_0/[M]_0 = 200$ and $[LA]_0 = 2.0$ M in benzene-d_6.

Time (h)	Conversion (%)	$[LA]_0/[LA]_t$
0	0	0
2	24	0.28
5	50	0.69
7	60	0.92
9	70	1.20
14	95	2.97
18	97	3.38
21	98	3.82

Table S22. *rac*-Lactide polymerisation using Pn*Zr(O-2,6-^{i}Pr-C_6H_3)$_2$ (**3**) at 80 °C with $[LA]_0/[M]_0 = 200$ and $[LA]_0 = 2.0$ M in benzene-d_6.

Time (h)	Conversion (%)	$[LA]_0/[LA]_t$
0	0	0
1	24	0.28
2	30	0.35
5	46	0.62
7	58	0.86
9	70	1.22
14	84	1.81
18	90	2.32
21	93	2.73
24	96	3.14
30	97	3.55

Table S23. *rac*-Lactide polymerisation using Pn*ZrCl(O-2,6-^{t}Bu-4-Me-C_6H_2) (**6**) at 80 °C with $[LA]_0/[M]_0 = 200$ and $[LA]_0 = 2.0$ M in benzene-d_6.

Time (h)	Conversion (%)	$[LA]_0/[LA]_t$
0	0	0
1	14	0.15
2	25	0.28
5	36	0.44
7	45	0.60
9	58	0.86
14	75	1.39
18	88	2.12
21	94	2.81
24	95	3.00

Table S24. *rac*-Lactide polymerisation using Pn*Zr(O-2,6-^{i}Pr-$C_6H_3)_2$ (**3**) at 60 °C with $[LA]_0/[M]_0 = 50$ and $[LA]_0 = 0.5$ M in benzene-d_6.

Time (h)	Conversion (%)	$[LA]_0/[LA]_t$
0	0	0
1	2	0.02
4	27	0.32
7	60	0.92
10	76	1.44

Table S25. *rac*-Lactide polymerisation using Pn*Zr(O-2,6-^{i}Pr-C_6H_3)$_2$ (**3**) at 70 °C with $[LA]_0/[M]_0 = 50$ and $[LA]_0 = 0.5$ M in benzene-d_6.

Time (h)	Conversion (%)	$[LA]_0/[LA]_t$
0	0	0
1	5	0.05
4	42	0.55
7	67	1.11
10	78	1.53

Table S26. *rac*-Lactide polymerisation using Pn*Zr(O-2,6-^{i}Pr-C_6H_3)$_2$ (**3**) at 80 °C with $[LA]_0/[M]_0 = 25$ and $[LA]_0 = 0.5$ M in benzene-d_6.

Time (h)	Conversion (%)	$[LA]_0/[LA]_t$
0	0	0
1	46	0.62
3	74	1.35
5	87	2.04
7	91	2.41

Table S27. *rac*-Lactide polymerisation using Pn*Zr(O-2,6-^{i}Pr-C_6H_3)$_2$ (**3**) at 80 °C with $[LA]_0/[M]_0 = 10$ and $[LA]_0 = 0.5$ M in benzene-d_6.

Time (h)	Conversion (%)	$[LA]_0/[LA]_t$
0	0	0
1	63	0.99
3	87	2.04
5	92	2.53

Table S28. *rac*-Lactide polymerisation using Pn*Zr(O-2,6-^{i}Pr-C_6H_3)$_2$ (**3**) at 80 °C with $[LA]_0/[M]_0 = 50$ and $[LA]_0 = 0.5$ M in benzene-d_6.

Time (h)	Conversion (%)	$[LA]_0/[LA]_t$
0	0	0
1	15	0.16
3	39	0.49
5	62	0.96
7	73	1.30
9	78	1.53

Table S29. *rac*-Lactide polymerisation using Pn*ZrCl(O-2,6-^{t}Bu-4-Me-C_6H_2) (**6**) at 80 °C with $[LA]_0/[M]_0 = 25$ and $[LA]_0 = 0.5$ M in benzene-d_6.

Time (h)	Conversion (%)	$[LA]_0/[LA]_t$
0	0	0
1	32	0.39
3	72	1.27
5	85	1.90
7	90	2.30

Table S30. *rac*-Lactide polymerisation using Pn*ZrCl(O-2,6-^{t}Bu-4-Me-C_6H_2) (**6**) at 80 °C with $[LA]_0/[M]_0 = 10$ and $[LA]_0 = 0.5$ M in benzene-d_6.

Time (h)	Conversion (%)	$[LA]_0/[LA]_t$
0	0	0
1	54	0.78
3	85	1.90
5	90	2.30

Table S31. *rac*-Lactide polymerisation using Pn*Zr(O-2,6-^{i}Pr-C_6H_3)$_2$ (**3**) at 80 °C with $[LA]_0/[M]_0 = 200$ and $[LA]_0 = 2.0$ M in chloroform-d_1.

Time (h)	Conversion (%)	$[LA]_0/[LA]_t$
0	0	0
1	2	0.02
4	41	0.52
9	60	0.92
16	84	1.82
20	93	2.61

Table S32. *rac*-Lactide polymerisation using Pn*ZrCl(O-2,6-^{t}Bu-4-Me-C_6H_2) (**6**) at 80 °C with $[LA]_0/[M]_0 = 200$ and $[LA]_0 = 2.0$ M in chloroform-d_1.

Time (h)	Conversion (%)	$[LA]_0/[LA]_t$
0	0	0
1	0	0
4	8	0.09
9	13	0.14
12	17	0.19
16	23	0.26

4.3 Homonuclear decoupled ^{1}H NMR spectra

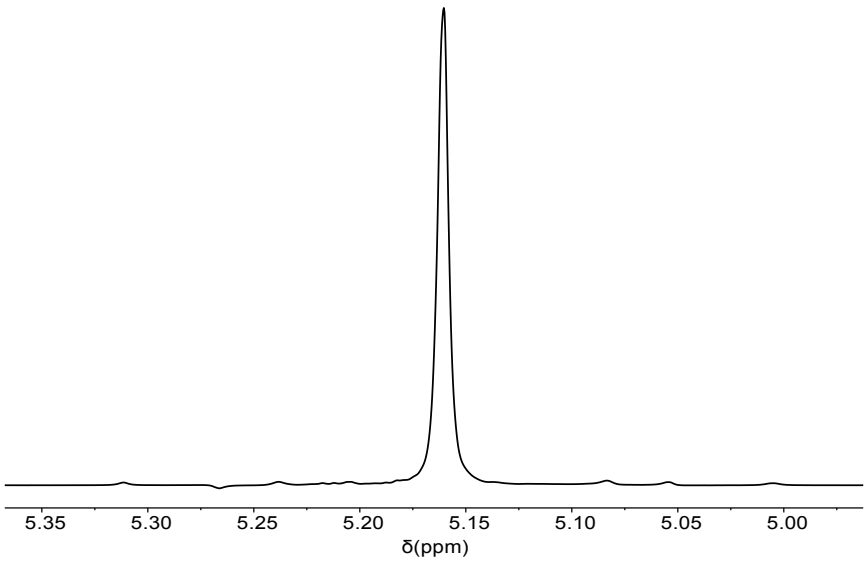

Fig. S35. $^{1}H\{^{1}H\}$ NMR spectrum (chloroform-d_1, 500 MHz, 298 K) of the poly-*L*-lactide produced using Pn*Zr(O-2,6-Me-$C_6H_3)_2$ (**2**). Polymerisation conditions: 80 °C, $[LA]_0/[M]_0 = 200$, $[LA]_0 = 2.0$ M and benzene-d_6.

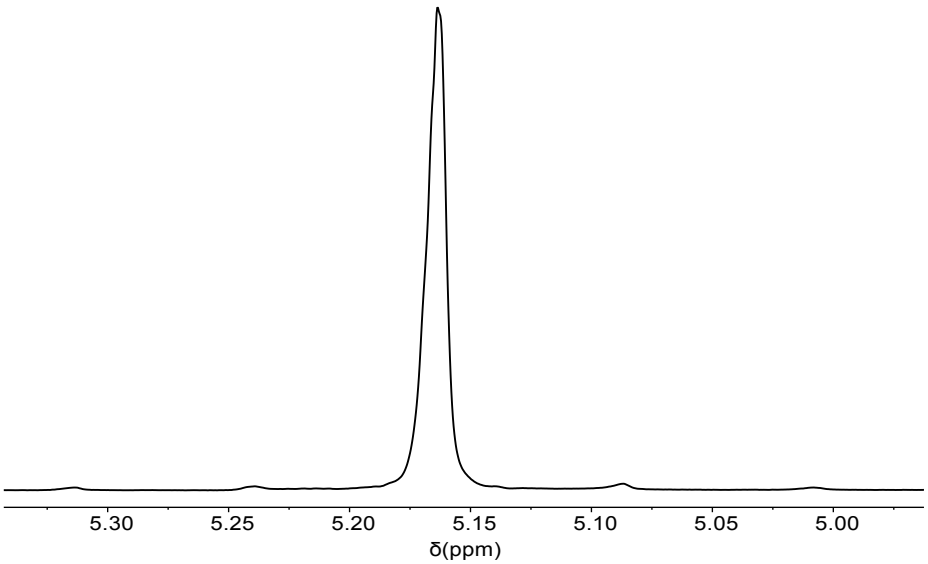

Fig. S36. $^{1}H\{^{1}H\}$ NMR spectrum (chloroform-d_1, 500 MHz, 298 K) of the poly-*L*-lactide produced using Pn*Zr(O-2,6-^{i}Pr-$C_6H_3)_2$ (**3**). Polymerisation conditions: 80 °C, $[LA]_0/[M]_0 = 200$, $[LA]_0 = 2.0$ M and benzene-d_6.

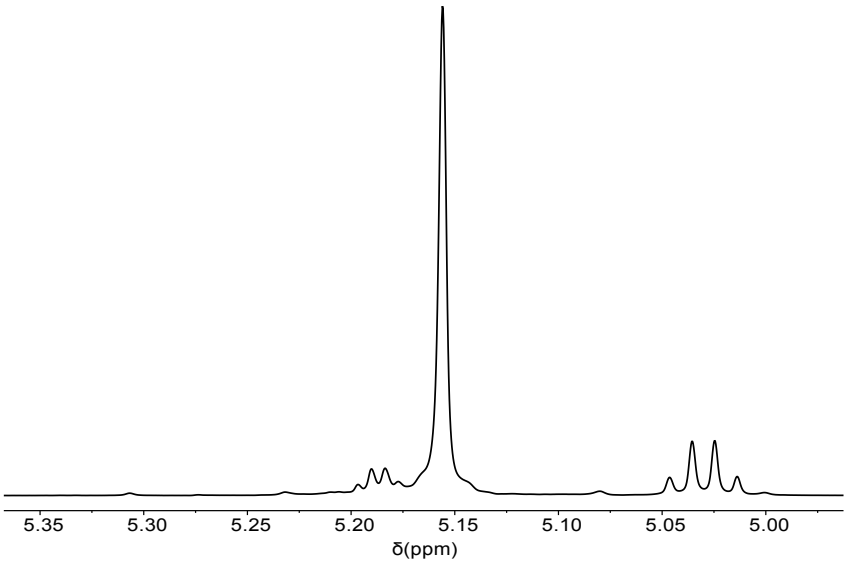

Fig. S37. $^{1}H\{^{1}H\}$ NMR spectrum (chloroform-d_1, 500 MHz, 298 K) of the poly-*L*-lactide produced using Pn*ZrCl(O-2,6-^{t}Bu-4-Me-C_6H_2) (**6**). Polymerisation conditions: 80 °C, $[LA]_0/[M]_0 = 200$, $[LA]_0 = 2.0$ M and benzene-d_6.

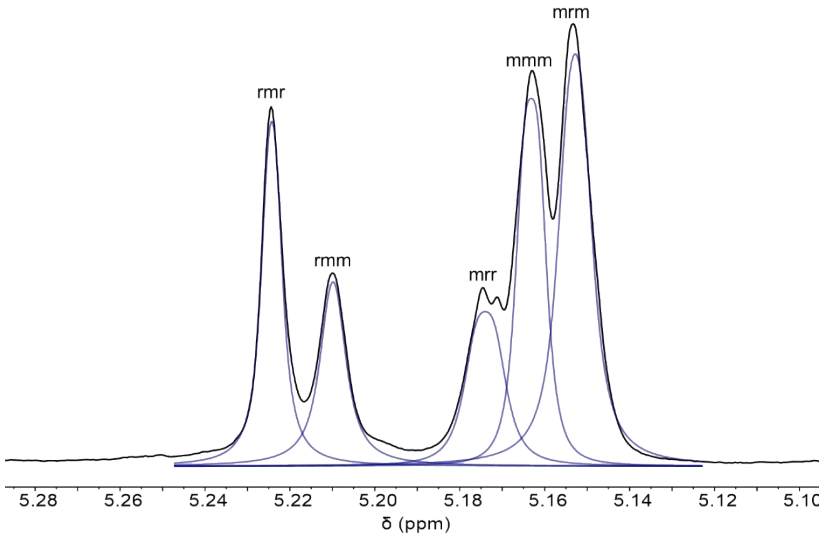

Fig. S38. $^{1}H\{^{1}H\}$ NMR spectrum (chloroform-d_1, 500 MHz, 298 K) of the poly-*rac*-lactide produced using Pn*Zr(O-2,6-Me-$C_6H_3)_2$ (**2**) (P_r = 0.66 ± 0.03). Polymerisation conditions: 80 °C, $[LA]_0/[M]_0 = 200$, $[LA]_0 = 2.0$ M and benzene-d_6.

Tetrad	Probability	P_r (deconvolution)
rmr	$P_r^2/2$	0.61
mmm	$P_m^2 + (P_rP_m)/2$	0.68
mrm	$(P_r^2 + P_rP_m)/2$	0.68
Average P_r		0.66 ± 0.03

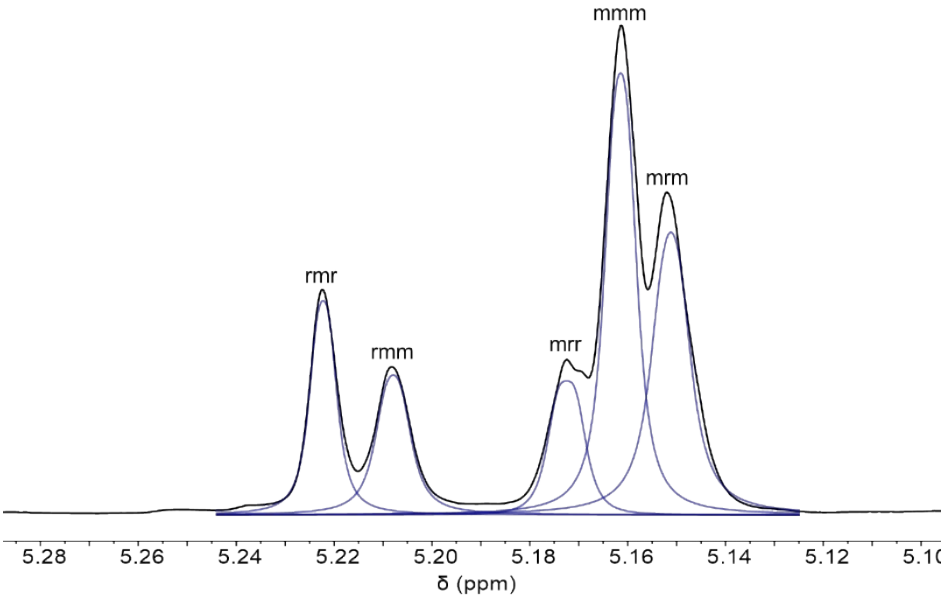

Fig. S39. $^{1}H\{^{1}H\}$ NMR spectrum (chloroform-d_1, 500 MHz, 298 K) of the poly-*rac*-lactide produced using Pn*Zr(O-2,6-Me-C_6H_3)$_2$ (**3**) (P_r = 0.54 ± 0.02). Polymerisation conditions: 80 °C, $[LA]_0/[M]_0$ = 200, $[LA]_0$ = 2.0 M and benzene-d_6.

Tetrad	Probability	P_r (deconvolution)
rmr	$P_r^2/2$	0.53
mmm	$P_m^2 + (P_rP_m)/2$	0.53
mrm	$(P_r^2 + P_rP_m)/2$	0.57
Average P_r		0.54 ± 0.02

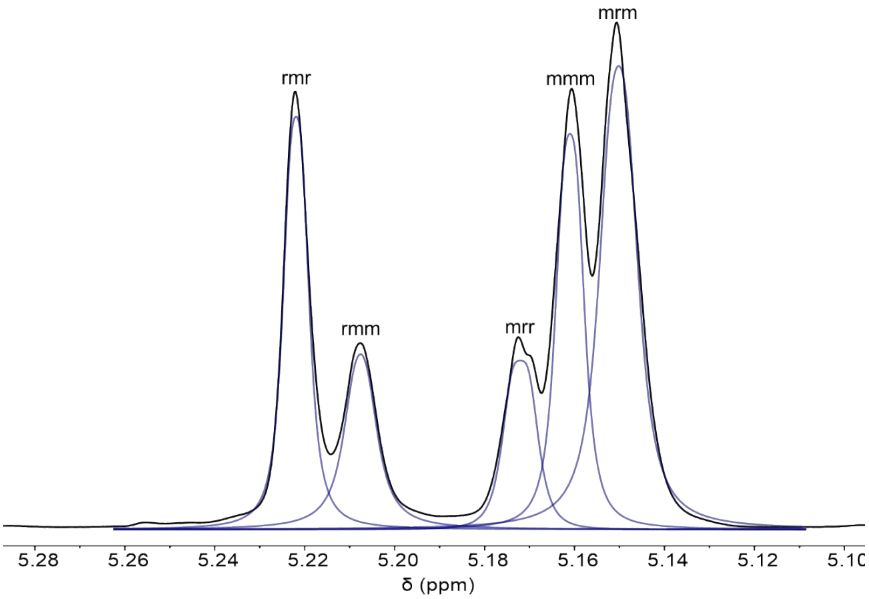

Fig. S40. $^{1}H\{^{1}H\}$ NMR spectrum (chloroform-d_1, 500 MHz, 298 K) of the poly-*rac*-lactide produced using Pn*ZrCl(O-2,6-^{t}Bu-4-Me-C_6H_2) (**6**) (P_r = 0.68 ± 0.03). Polymerisation conditions: 80 °C, $[LA]_0/[M]_0$ = 200, $[LA]_0$ = 2.0 M and benzene-d_6.

Tetrad	Probability	P_r (deconvolution)
rmr	$P_r^2/2$	0.64
mmm	$P_m^2 + (P_rP_m)/2$	0.68
mrm	$(P_r^2 + P_rP_m)/2$	0.71
Average P_r		0.68 ± 0.03

4.4 MALDI-TOF mass spectra

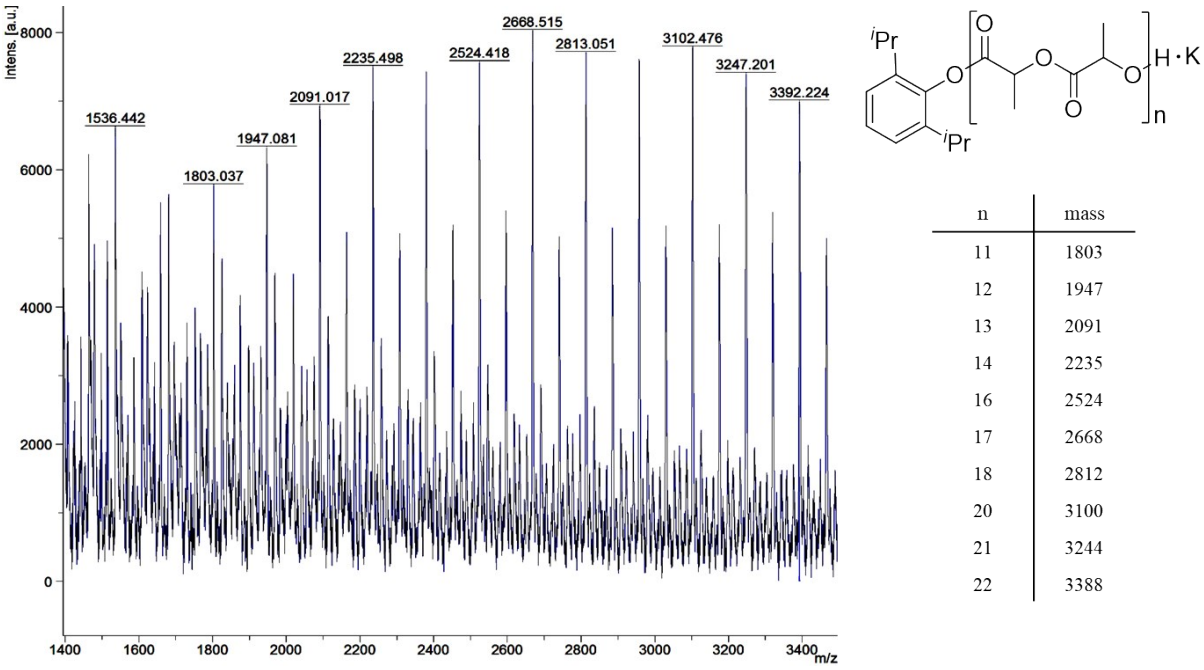

n	mass
11	1803
12	1947
13	2091
14	2235
16	2524
17	2668
18	2812
20	3100
21	3244
22	3388

Fig. S41. MALDI-TOF mass spectrum (recorded in a DCTB + KTFA matrix) of the poly-*rac*-lactide synthesised using Pn*Zr(O-2,6-^{i}Pr-C_6H_3)$_2$ (**3**). Polymerisation conditions: 80 °C, $[LA]_0/[M]_0 = 10$, $[LA]_0 = 0.5$ M and benzene-d_6.

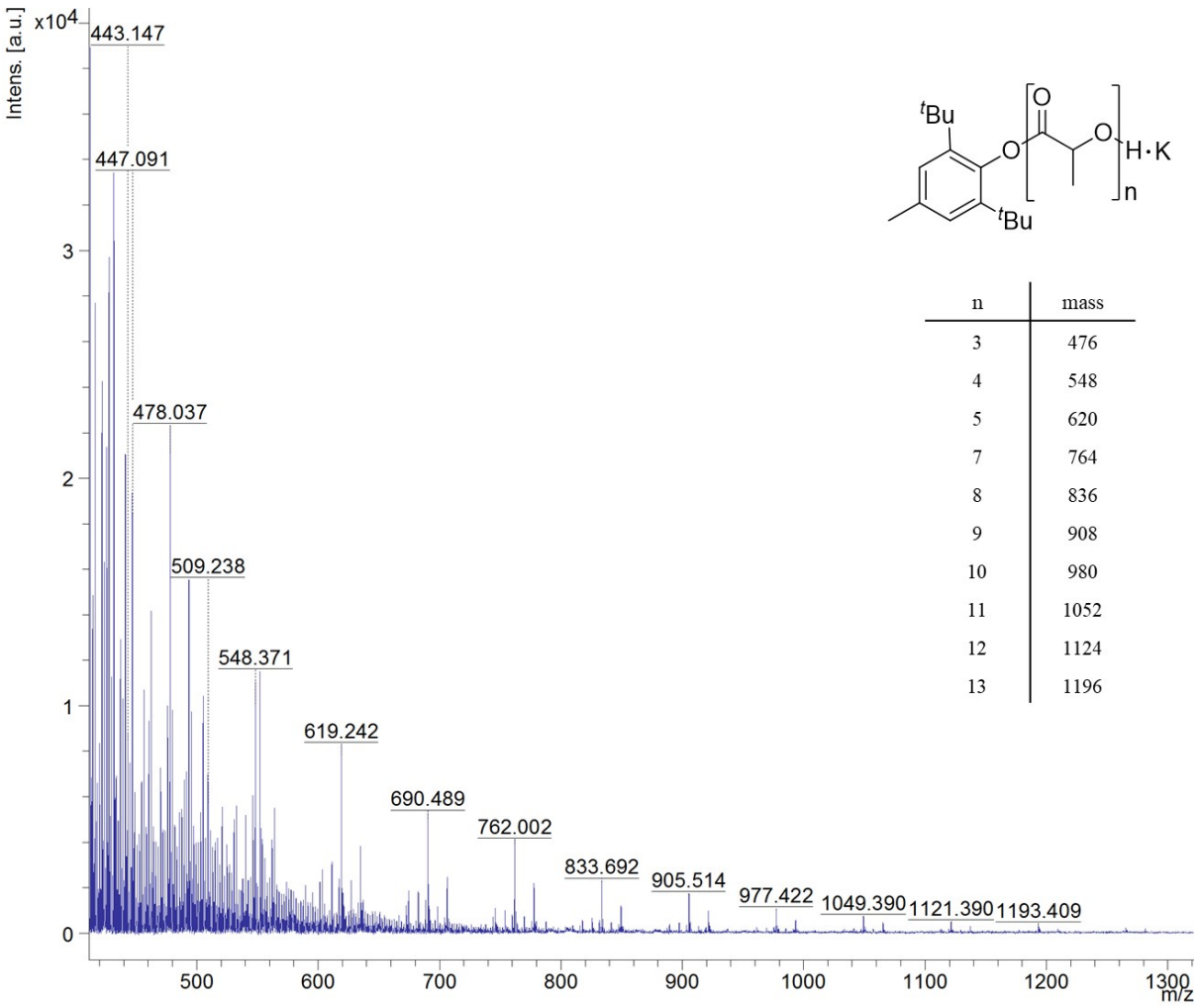

n	mass
3	476
4	548
5	620
7	764
8	836
9	908
10	980
11	1052
12	1124
13	1196

Fig. S42. MALDI-TOF mass spectrum (recorded in a DCTB + KTFA matrix) of the poly-*rac*-lactide synthesised using Pn*ZrCl(O-2,6-^{t}Bu-4-Me-C_6H_2) (**6**). Polymerisation conditions: 80 °C, $[LA]_0/[M]_0 = 10$, $[LA]_0 = 0.5$ M and benzene-d_6.

5. References

1. R. T. Cooper, F. M. Chadwick, A. E. Ashley and D. O'Hare, *Organometallics*, 2013, **32**, 2228-2233.
2. F. M. Chadwick, R. T. Cooper, A. E. Ashley, J.-C. Buffet and D. M. O'Hare, *Organometallics*, 2014, **33**, 3775-3785.
3. D. A. X. Fraser, Z. R. Turner, J.-C. Buffet and D. O'Hare, *Organometallics*, 2016, **35**, 2664-2674.
4. T. J. Boyle, N. L. Andrews, M. A. Rodriguez, C. Campana and T. Yiu, *Inorg. Chem.*, 2003, **42**, 5357-5366.
5. M. J. Monreal, R. K. Thomson, T. Cantat, N. E. Travia, B. L. Scott and J. L. Kiplinger, *Organometallics*, 2011, **30**, 2031-2038.
6. P. A. Evans and A. L. Stanley, *Synthetic Communications*, 1995, **25**, 515-519.
7. M. Save, M. Schappacher and A. Soum, *Macromol. Chem. Phys.*, 2002, **203**, 889-899.
8. J. Cosier and A. M. Glazer, *J. Appl. Crystallogr.*, 1986, **19**, 105-107.
9. CrysAlisPRO, Oxford Diffraction /Agilent Technologies UK Ltd, Yarnton, England.
10. (a) A. Altomare, G. Cascarano, C. Giacovazzo and A. Guagliardi, *J. Appl. Crystallogr.*, 1993, **26**, 343-350; (b) Sheldrick, G. M., *Acta Crystallogr., Sect. A: Found. Adv.,* 2008, **64**, 112-122; (c) Sheldrick, G. M., *Acta Cryst., Sect. C: Struct. Chem.,* 2015, **71**, 3-8
11. L. Palatinus and G. Chapuis, *J. Appl. Crystallogr.*, 2007, **40**, 786-790.
12. L. Farrugia, *J. Appl. Crystallogr.*, 1999, **32**, 837-838.
13 Otwinowski, Z.; Minor, W. *Methods Enzymol.* **1997**, *276*, 307.
14 Blessing, R. H. *Acta Crystallogr. Sect. A* **1995**, *51*, 33.